Journal of Orthopaedic Translation 42 (2023) 57–72

Contents lists available at ScienceDirect

Journal of Orthopaedic Translation

journal homepage: www.journals.elsevier.com/journal-of-orthopaedic-translation

Magnetic resonance imaging techniques for the quantitative analysis of skeletal muscle: State of the art

Klaus Engelke [a,b,d,*], Oliver Chaudry [a], Lena Gast [e], Mootaz AB. Eldib [c], Ling Wang [f], Jean-Denis Laredo [g], Georg Schett [a], Armin M. Nagel [e,h]

[a] Department of Medicine III, Friedrich-Alexander University of Erlangen-Nürnberg, University Hospital Erlangen, Ulmenweg 18, 91054, Erlangen, Germany
[b] Institute of Medical Physics (IMP), Friedrich-Alexander-Universität Erlangen-Nürnberg (FAU), Henkestr. 91, 91052, Erlangen, Germany
[c] Clario Inc, USA
[d] Clario Inc, Germany
[e] Institute of Radiology, Friedrich-Alexander-Universität Erlangen-Nürnberg (FAU), University Hospital Erlangen, Maximiliansplatz 3, 91054, Erlangen, Germany
[f] Department of Radiology, Beijing Jishuitan Hospital, Beijing, China
[g] Service d'Imagerie Médicale, Institut Mutualiste Montsouris & B3OA, UMR CNRS 7052, Inserm U1271 Université de Paris-Cité, Paris, France
[h] Division of Medical Physics in Radiology, German Cancer Research Center (DKFZ), Im Neuenheimer Feld 280, 69120, Heidelberg, Germany

ARTICLE INFO

Keywords:
Clinical trials
Dixon
Diffusion tensor imaging
Muscle MRI
T2 mapping
Quantitative analysis

ABSTRACT

Background: Magnetic resonance imaging (MRI) is the dominant 3D imaging modality to quantify muscle properties in skeletal muscle disorders, in inherited and acquired muscle diseases, and in sarcopenia, in cachexia and frailty.

Methods: This review covers T1 weighted and Dixon sequences, introduces T2 mapping, diffusion tensor imaging (DTI) and non-proton MRI. Technical concepts, strengths, limitations and translational aspects of these techniques are discussed in detail. Examples of clinical applications are outlined. For comparison ^{31}P-and ^{13}C-MR Spectroscopy are also addressed.

Results: MRI technology provides a rich toolset to assess muscle deterioration. In addition to classical measures such as muscle atrophy using T1 weighted imaging and fat infiltration using Dixon sequences, parameters characterizing inflammation from T2 maps, tissue sodium using non-proton MRI techniques or concentration or fiber architecture using diffusion tensor imaging may be useful for an even earlier diagnosis of the impairment of muscle quality.

Conclusion: Quantitative MRI provides new options for muscle research and clinical applications. Current limitations that also impair its more widespread use in clinical trials are lack of standardization, ambiguity of image segmentation and analysis approaches, a multitude of outcome parameters without a clear strategy which ones to use and the lack of normal data.

1. Introduction

Magnetic resonance (MR) is an established technique for imaging skeletal muscle disorders. Traditionally, MR sequences sensitive to water such as T1-weighted images (T1w), short-tau inversion recovery (STIR) or T2-weighted images (T2w) with or without fat suppression have been used to determine progression and treatment effects in inherited and acquired muscle diseases [1–5]. Typically, semi quantitative scores such as Mercury [6,7], Jungbluth [8], Lamminen [9] Goutallier [10,11] or Poliachik [12], were used to grade structural integrity, fatty muscle infiltration, muscle edema and MR signal intensity.

Predominant locations were muscles of the lower extremities, which are large and relatively easy to assess. Chemical shift imaging sequences [13] to quantify fat infiltration and T1w imaging [14] have been explored in the last century to allow earlier detection of muscle diseases compared to the use of semi quantitative scores. In 2009 and 2010 two TREAT-NMD (https://treat-nmd.org/) workshops on skeletal muscle MRI recommended the use of "whole body T1w imaging, for the screening of disease extension, Dixon imaging with water–fat separation, for the quantitation of fatty infiltration and parametric T2 imaging, for the quantitation of inflammation" as outcome measures for

* Corresponding author. Department of Medicine III, Friedrich-Alexander University of Erlangen-Nürnberg, University Hospital Erlangen, Ulmenweg 18, 91054, Erlangen, Germany.
E-mail address: Klaus.Engelke@fau.de (K. Engelke).

https://doi.org/10.1016/j.jot.2023.07.005
Received 17 February 2023; Received in revised form 4 July 2023; Accepted 19 July 2023

Abbreviations

ADC	apparent diffusion coefficient
AT	adipose tissue
BMI	body mass index
CT	computed tomography
DMD	Duchenne muscular dystrophy
DWI	diffusion weighted imaging
DTI	diffusion tensor imaging
DXA	dual X-ray absorptiometry
EMCL	extra myocellular lipids
FA	fractional anisotropy
FF	fat fraction
IMAT	intermuscular adipose tissue
IMCL	intra myocellular lipids
MD	mean diffusivity
MR	magnetic resonance
MRE	MR elastography
MRI	magnetic resonance imaging
MRS	magnetic resonance spectroscopy
MT	muscle tissue
NMD	neuromuscular disease
PDFF	proton density fat fraction
PDWF	proton density water fraction
SAT	subcutaneous adipose tissue
SE	spine echo
STIR	short-tau inversion recovery MRI sequence
T1w	a specific so called T-weighted MRI sequence
T2w	a specific so called T2-weighted MRI sequence
TMS	tetramethylsilane
wb-MRI	whole body MRI

neuromuscular diseases (NMD) [15]. New MR imaging and spectroscopy techniques for NMD were also summarized in a workshop report of a funded COST action project (co-operation in science and technology) of the European Union "BM1304 MYO-MRI" [16].

In the last two decades interest in muscle imaging has been extended to muscle atrophy or muscle wasting caused by or associated with inactivity, denervation, fasting, malnutrition, chronic obstructive pulmonary disorder, cancer-associated cachexia, diabetes, renal failure, cardiac failure, Cushing syndrome, sepsis, burns and trauma [17]. Further areas of interest are the association of quantitative muscle parameters with back pain [18–21], myosteatosis [22] and sarcopenia [23,24]. The interdependence of myosteatosis and inflammation that propagates tissue degeneration is increasingly been recognized as an important component of aging and frailty [25,26].

The focus of this contribution is on technical aspects of quantitative MR techniques currently used to image skeletal muscle. Imaging of muscle perfusion and imaging of smooth and cardiac muscle is not considered. For comparison, a section on MR spectroscopy (MRS) is included. A comprehensive review of medical applications is beyond the scope of this article, only selected examples can be illustrated. Muscle size/volume and fat infiltration can also be measured with computed tomography (CT). One recent focus of muscle CT was on the prediction of osteoporotic fractures [27–32]. Techniques of quantitative muscle CT were covered by an earlier review [33].

2. Muscle fat infiltration

In muscle, lipids are either stored as adipocytes, with fat imaging characteristics, or as intramyocellular lipid droplets (IMCL: intramyocellular lipids). Adipocytes can be located sub fascial between muscle groups (perimuscular adipose tissue), or as interstitial (intramuscular) adipose tissue within an individual muscle as extramyocellular lipids (EMCL) (Fig. 1). T1w images provide good contrast between muscle and adipose tissue but IMCL and smaller EMCL aggregations are not visible in the T1w images.

Historically, in the thigh the combination of all visible adipose tissue (AT) below the deep fascia, be it perimuscular AT or larger EMCL aggregations has been denoted as intermuscular adipose tissue (IMAT) [25,34]. Unfortunately, the term IMAT is used inconsistently throughout the literature. A different definition of IMAT was given in a recent Interdisciplinary Workshop at the National Institute on Aging, which stated that myosteatosis included three components "(a) intermuscular adipose tissue (IMAT), the extra-myocellular adipose tissue found beneath the fascia and in-between muscle groups; (b) intramuscular adipose tissue, the extramyocellular adipose tissue found within an individual muscle; and (c) intramyocellular lipids (IMCL)" [35]. According to this definition, IMAT is equivalent to perimuscular AT as shown in Fig. 1 but does not include any intramuscular adipose tissue. Standardization of terminology is needed. In this contribution we will use IMAT in the traditional way and will divide the tissue beneath the fascia into IMAT, which in T1w images appears bright and muscle tissue (MT), which appears dark.

From an anatomical and physiological perspective muscle tissue is the contractile tissue, composed of cells, which can shorten or contract. This definition excludes all EMCLs. However, due to limited spatial resolution of in vivo imaging small EMCL aggregations cannot be visualized and cannot be separated from the contractile tissue. Thus, the term MT used in imaging is usually less strict as MT will contain smaller aggregations of non-contractile EMCL.

Skeletal muscle fat infiltration which is also known as myosteatosis [35] differs from sarcopenia, which according to the more recent definitions focusses on external muscle function, whereas myosteatosis focusses on the internal muscle property of fat infiltration [22].

3. MR spectroscopy

MRS of skeletal muscle is primarily used to assess the muscle metabolism using ^{31}P-MRS or ^{13}C-MRS to measure concentrations of high energy phosphates or muscular glycogen, respectively, or using ^{1}H-MRS to assess the muscle lipid composition [36–38]. An excellent summary of ^{31}P- and ^{13}C-MRS [16] and consensus recommendations for ^{31}P-MRS of skeletal muscle [39] have recently been published. ^{1}H-MRS generates an intensity spectrum as a function of relative chemical shifts of lipid metabolites measured in ppm versus the universal reference, the methyl ^{1}H signal of tetramethylsilane (TMS), which is assigned a value of 0 ppm [40]. In this reference system water protons in living tissues resonate at ~4.7 ppm, EMCL at ~1.5 ppm and IMCL at ~1.28 ppm.

In MR imaging the chemical shift between water and fat is either used to suppress the fat signal and to selectively excite the water signal or for example in Dixon imaging (see section 6.2) to separate fat and water signals. However, very small chemical shift difference of ~0.2 ppm between EMCL and IMCL as well as between other liquid metabolites cannot be detected by Dixon imaging [36,41]. In contrast, MRS allows for a differentiation of IMCL and EMCL despite their similar chemical composition, due to small susceptibility effects of structural differences between the more spherical lipid droplets (IMCL) and the plate- or tube-like structures of EMCL [42]. The detection of these differences requires long acquisition times, thus the MRS signal is typically obtained from a small (≈1 cm^3) volume of interest, the so-called spectroscopy voxel. Consensus recommendations on how to perform ^{1}H-MRS in skeletal muscle have been published recently [43].

One main difficulty of MRS is the repositioning of the spectroscopic voxel in the same anatomical location. Muscle is an elastic tissue and the

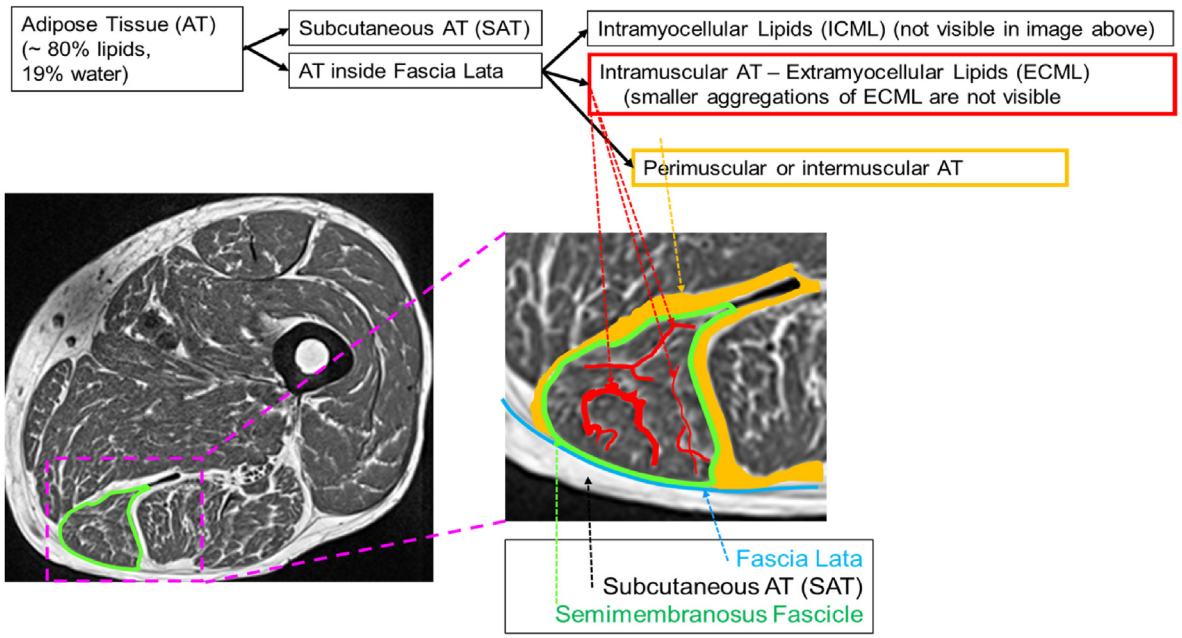

Fig. 1. Muscle fat infiltration shown schematically in the semimembranosus of the mid-thigh. The T1w image provides good contrast and shows the individual muscles separated by perimuscular adipose tissue (orange) and intramuscular adipose tissue (red). However, the amount of visible intramuscular adipose tissue depends on the spatial resolution and smaller aggregations of intramuscular adipose tissue either cause partial volume artifacts or cannot be detected in T1w images at all. The muscle tissue (dark) contains contractile tissue, and lipids, either as EMCLs and IMCLs that contribute to the fat faction signal in Dixon images. (For interpretation of the references to color in this figure legend, the reader is referred to the Web version of this article.)

high and inhomogeneous muscle fat infiltration present in elderly and diseased subjects further complicates the reproducible positioning. This results in poorer precision compared to Dixon imaging (see section 6.2).). For comparison, precision is much less problematic in the liver, another organ for which Dixon imaging is frequently used, because liver is a more homogeneous tissue than skeletal muscle. A solution could be MRS imaging but applications in muscle are still rare [44–46].

^{1}H-MRS has been used in muscular dystrophies but is increasingly been replaced by Dixon imaging and T2 mapping [47–50]. Quantification of IMCLs is a powerful tool in exercise and nutrition research, for bioenergetics studies and for studies of insulin resistance [36,51].

4. MR imaging

4.1. T1 weighted sequences

T1w fast spin echo (SE) sequences have long been the dominant sequence in muscle imaging as they provide excellent contrast between muscle and adipose tissue (Fig. 2a), which is the basis for qualitative or semi quantitative radiological assessments. In combination with appropriate segmentation, T1w images are also used for the quantitative measurement of area or volume of tissue compartments such as subcutaneous adipose tissue (SAT), IMAT or MT. Compared to gradient echo sequences, SE sequences are less sensitive to susceptibility artifacts that can arise from fatty inflation. SE T1w sequences can be obtained with good spatial resolution ($0.5 \times 0.5 \times 3$ mm^3) and in extremities a stack of 30 images can be obtained in less than 5 min (Table 1). The intensity values of T1w images vary among sequences and manufacturers. They can be used to guide the segmentation but they are of limited value with regard to other quantitative measurements.

T1w sequences are standard sequences, available on all MR scanners and easy to use. They are still a good choice for measurement of muscle volume and semiquantitative assessment of muscle fat infiltration, although this is also the realm of computed tomography, which due to faster scan times is less sensitive to motion artifacts. Whole body MRI (wb-MRI) sequences originally developed for oncologic screening are of interest for myopathies affecting a large variety of muscles throughout the body [52–54]. For such a scan, typically multiple coils are used to cover the whole body. As an alternative, separate scans along the body are stitched together.

4.2. Dixon imaging

T1w cannot be used to quantify muscle fat infiltration. This is the realm of Dixon techniques. If the advanced imaging and signal processing techniques described in the Technical Appendix are used to correct for confounding factors, Dixon techniques deliver parametric water and fat maps denoted as ‘proton density fat fraction’ (PDFF) and ‘proton density water fraction’ (PDWF) maps. ‘PDFF is defined as the ratio of density of mobile protons from fat (triglycerides) and the total density of protons from mobile triglycerides and mobile water’. PDFF reflects tissue fat concentration and correlates with tissue triglyceride concentration but is not equivalent to mass fat fraction. PDFF has been suggested to be used as standardized MRI and MRS parameter to measure the tissue fat concentration [55]. Conversion of PDFF to absolute fat mass in grams has been reported [56]. For a given voxel, PDFF + PDWF = 1, as only water and fat protons contribute to the measured MR signal. In the presence of edema or fibrosis, PDWF differs from the absolute water content.

Depending on scanner model, intensity values of the PDFF map scale from 1 to 100 or from 1 to 1000 and linearly code the fat fraction from 1% to 100% or from 0.1 to 100%, respectively. An intensity range from 1 to 1000 provides higher sensitivity as PDFF differences of 0.1% can be resolved. In principle, tissue specific differences of the triglyceride spectrum have to be considered in the signal models of the advanced Dixon techniques but spectral differences observed in nonalcoholic steatohepatitis for example, had little impact on PDFF outcome [57]. In humans the triglyceride composition of subcutaneous adipose tissue and bone marrow did not differ for a given subject [58]. Nevertheless, the impact of differences in the triglyceride spectra of muscle and liver should be further investigated as most manufacturer implemented Dixon sequences used for muscle assessments are optimized for the liver.

In the liver multiple studies have reported PDFF accuracy [59] but

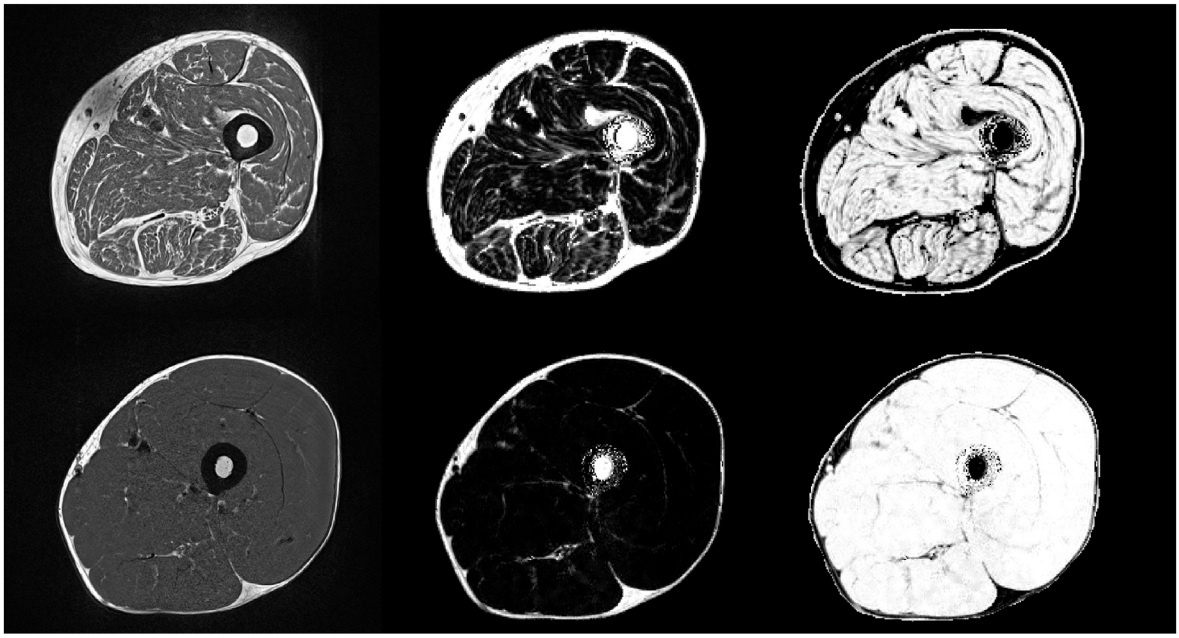

Fig. 2. T1w images of elderly subject with sarcopenia (top) and of young healthy subject (bottom). A: T1 weighted sequence, B: Dixon fat fraction sequence and C: Dixon water fraction sequence. The T1w image in A is affected by bias (upper left corner of the image in the upper row), Dixon fat and water images are also affected but this effect cancels out the PDFF and PDFW images (upper row B and C).

Table 1
Representative values of spatial resolution and acquisition time for MRI sequences for a 10 cm long scan of the mid thigh. Values apply to 1.5 and 3 T MRI scanners; for 1.5 T scanners similar values apply. Please note: covering 10 cm with T2 mapping and DTI using 5 slices with a thickness of 10 mm implies a gap of 10 mm between slices*values for 7 T scan of the calf.

Sequence	Resolution [mm^3]	No of slices	Acquisition time [min]	Typical applications
T1w	0.5 × 0.5 x 3.0	36	3–5	quantification of muscle volume and atrophy in sarcopenia and cachexia, semiquantitative assessment of fat infiltration in muscle myopathies
Dixon	1.6 × 1.6 x 3.0	36	0.5–1	quantification of muscle fat infiltration in muscle myopathies and for body composition
Dixon high res.	0.8 × 0.8 x 3.0	36	1–2	
T2 map (10 echos)	1.3 × 1.3 x 10.0	5	2–4	quantification of muscle edema in muscle myopathies, muscle injury and exercise
T2 map (32 echos)	1.3 × 1.3 x 10.0	5	3–6	
DTI	1.3 × 1.3 x 10.0	5	4–6	quantification of muscle fiber architecture in exercise and muscle myopathies
39 K (AW-SOSt)*	7.5 × 7.5 x 30	8	8-10	experimental
23Na (AW-SOSt)*	2.5 × 2.5 x 15	16	8-10	experimental

studies in skeletal muscle are rare. PDFF accuracy is typically reported as correlation and bias between Dixon and MRS measurements where MRS serves as gold standard. Correlations between 6 pt Dixon and MRS of $r \geq 0.95$ and absolute differences in FF of $\leq$5% have been reported in vivo [60,61]. Absolute differences in FF among a variety of 2 pt, 3 pt, and 6 pt Dixon sequences implemented on a Siemens 3 T MAGNETOM Skyrafit were $\leq$4.5% with the exception of much higher inaccuracies of a 2 pt Dixon sequence that did not use exact in (2.4 ms) and out of phase (1.2 ms) echo times [62].

Dixon sequences have become the method of choice to quantify muscle fat infiltration. However, it is a limitation that IMCL and EMCL cannot be separated thus PDFF results contain contributions form IMCL that are vital for the energy metabolism of the cell, whereas fatty muscle infiltration attributable to EMCL has a negative impact on muscle function. Acquisition of Dixon images is faster than of T1w images (Table 1) but typically spatial resolution is inferior. Thus T1w images are often preferred over Dixon images for assessment of muscle volume and for muscle segmentation, although Dixon images can also be used for these tasks. As a disadvantage to Dixon, T1w images may be affected by bias (Fig. 2a) causing an inhomogeneous contrast across the images, which cancels out in the Dixon images.

Recently, whole body Dixon MRI has been developed for body composition studies [63–66] as an alternative to whole body dual X-ray absorptiometry (DXA). In contrast to DXA, with a 3D imaging technique such as Dixon MRI, fat and water fractions of individual organs and muscles can be quantified separately. However, it should be considered whether separate MR acquisitions that can be optimally adapted to a given anatomical region are advantageous to a whole body MRI scan [67].

4.3. T2 maps

In addition to PDFF, T2 relaxation times are increasingly used as a quantitative MR marker for disease activity in skeletal muscle tissue in part replacing STIR sequences that have been used for semiquantitative assessment of edema [68,69]. Skeletal muscle edema can be caused by trauma and is also observed in early myositis ossificans and inflammatory myopathies. Edema results in increased muscular T2 relaxation times and is an indicator for inflammatory processes, which often precede the replacement of muscle tissue by adipose tissue [70]. Alterations in T2 are generally non-specific, however, they can represent the intensity of underlying pathological changes [71]. To assess T2 in skeletal muscles, multi-spin-echo (MSE) sequences are commonly used. Different fitting approaches have been proposed to evaluate the resulting signal evolution

and determine the T2 relaxation times.

The simplest approach is to fit a mono-exponential signal decay (Figure-A 1), which results in an overall, so-called "global T2 relaxation time" [71]. This global T2 represents an average of all compartments within the muscle, containing both muscle and adipose tissue. It highly depends on the amount of fat infiltration, as lipids possess significantly longer T2 times than (muscle) water. For example, at 3 T, T2 of muscle water ($T2_{water}$) in the range of 25–30 ms and T2 of fat ($T2_{fat}$) of approx. 150 ms have been reported [72]. Thus, an enhanced intramuscular FF results in an increased global T2 [73]. This effect is particularly prominent in subjects with a high amount of intramuscular fat such as patients with neuromuscular disorders [73,74]. Increases in global T2 due to fat infiltration may even mask actual pathological changes in $T2_{water}$, which are usually relatively small (approx. 10 ms) [71].

Different approaches have been proposed to selectively determine the T2 of muscle water in the presence of fat infiltration. For example, the water signal can be selectively excited or the signal of fat can be suppressed using conventional fat suppression techniques [70,75]. However, the quality of fat suppression usually relies on correct flip angles and therefore fails in regions of an inhomogeneous transmit (B1+) field. Another approach is multi-exponential T2 fitting [73] described in detail in the Technical Appendix.

4.4. Diffusion weighted imaging

Diffusion-weighted imaging (DWI) maps the thermal energy related random motion of water molecules. Outcome is the water diffusion rate [76]. However, in a tissue like muscle impermeable or semi permeable walls around the muscle fibers and other structures restrict the diffusion of molecules. This restriction is anisotropic. In mathematical terms it is described by a 3×3 matrix called the diffusion tensor D as described in detail in the Technical Appendix. Diffusion tensor imaging (DTI) [77] is an extension of DWI to determine the degree of anisotropy of the diffusion. Further outcomes of DTI are the mean diffusivity (MD) also termed apparent diffusion coefficient (ADC) and the fractional anisotropy FA as described in more detail in the Technical Appendix. DTI is an important technique for quantification of muscle fiber architecture because water diffusivity in the axial muscle fiber directions higher than in the radial fiber direction [78,79]. ADC and FA values for various muscles have been published [80–83]. In edematous muscle diffusivity in both, axial and radial directions, and FA are increased compared to healthy muscle [82–84] indicating the relevance of DTI in inflammatory myopathies [83,85], although no effect of myositis on ADC or FA has been observed in a recent study [86]. Discrepancies have also been reported in patients with Duchenne Muscular Dystrophy (DMD): higher ADC and lower FA values compared to healthy subjects in one [87] and opposite effects in other studies [81,88]. Reasons are lower ADC in adipose tissue compared to skeletal muscle [79,85] and impact of noise on FA values [78,89]. Consequently, it has been suggested to combine assessments of water T2, PDFF and signal to noise ratio for a correct interpretation of DTI measures [90].

For DTI image acquisition typically a single-shot diffusion weighted SE echo planar imaging (EPI) pulse sequence is used. As described above, DTI assessments are affected by the amount of adipose tissue, thus fat suppression is required in DTI. Accuracy further depends on acquisition parameters such as TE, TR or voxel size and age, sex or BMI. Further details have been addressed in recent reviews [91–93].

DTI is still not widely used for or muscle imaging. Examples in addition to myopathies discussed above are changes in muscle diffusivity associated with denervation [94], metabolic disease [95,96] muscle fiber tears [97,98], and differences in muscle diffusivity between osteoporotic and osteoarthritic subjects [99]. Another interesting field is the relation between muscle properties and external muscle strength that has important implications for optimizing training effects in athletes and for exercise or pharmaceutical interventions in sarcopenia and frailty [100–106].

Given adequate image quality of the DTI dataset [92,107] special algorithms can be applied to visualize the 3D muscle fiber architecture (Figure-A 2) or to be more accurate, to visualize the diffusivity in the axial muscle fiber direction. With this method termed tractography also parameters such as pennation angle, fiber length and curvature, and physiological cross-sectional area, which is the muscle area perpendicular to its fibers, can be quantified. Obviously, interpretation of results must consider that fiber tractography is not a real representation of muscle structure but a computational estimation. Applications of tractography in muscles are still rare [108–112]. However, 3D fiber tractography used in trunk or leg muscles may have great potential in assessing the risk of falls and related fractures.

4.5. Non-proton MRI methods

Non-proton MRI techniques can provide valuable insights into the composition of muscle tissue [113]. For example, ^{23}Na MRI enables the quantitative measurement of the tissue sodium concentration (TSC), and, thus can provide important information about the tissue ion homeostasis. One of the main regulators of the tissue ion homeostasis is the Na^+/K^+-ATPase (or Na^+/K^+-pump). In healthy tissue, the Na^+/K^+-ATPase helps to maintain a concentration gradient between intra- ($[Na^+]_{in}$ = 10–15 mmol/L) and extracellular sodium ($[Na^+]_{ex}$ = 145 mmol/L), which is of utmost importance for the excitation and inhibition of muscle cells.

The TSC is a volume-weighted average of intra- and extracellular sodium concentrations. For healthy muscle tissue, a mean intracellular volume fraction of approximately 0.92 can be assumed [114]. This results in a TSC of 21–25 mmol/L. Changes of the intracellular sodium concentration, or slight changes of the intracellular volume-fraction can result in large TSC changes, which can be assessed by ^{23}Na MRI. In addition to TSC measurements, relaxation-weighted ^{23}Na MRI techniques such as ^{23}Na inversion recovery MRI can be applied to achieve a weighting of the contrast towards the intracellular sodium [115]. ^{23}Na MRI of skeletal muscle tissue has been applied in several clinical research studies [115–117]. For instance, sodium anomalies were observed in patients with DMD, and were present even in absence of fatty degenerative changes and water T2 increases [118].

Using dedicated ultra-high field MRI systems ($B_0 \geq 7$ T), also other ions such as potassium or chloride can be investigated using ^{39}K or ^{35}Cl MRI to provide a more comprehensive analysis of the tissue ion homeostasis [119,120]. However, so far, ^{35}Cl and ^{39}K MRI of skeletal muscle tissue have only been performed in small feasibility studies [121–123].

4.6. MR elastography

In clinical practice, the manual examination of palpation is frequently used for the qualitative assessment of biomechanical tissue properties. MR elastography (MRE) enables quantitative evaluation of these biomechanical tissue properties. In MRE, shear waves that are typically introduced by a vibrating actuator, are imaged with a motion-sensitive MRI sequence [124]. A detailed description of principles and guidelines for MR elastography can be found in Ref. [125]. Applications of MRE to skeletal muscle research has recently been summarized [16]. For example, it has been shown that altered elastic properties of dystrophic muscle of patients with DMD can be detected by MRE [126,127].

5. Muscle analysis and quantitative parameters

5.1. Muscle segmentation

Quantitative muscle measurements such as fat fraction, or T2 water require a prior segmentation. The general trend from analysis of single towards analysis of multiple slices, for example covering the whole thigh, requires a higher degree of automation to limit overall operator efforts. A

number of muscle segmentation algorithms have been developed in particular for NMD [128,129] but comparison of performance is difficult because of differences in acquisition parameters, sequences and assessments. One strategy used in subjects with sarcopenia, is to segment the *fascia lata* (of the thigh) or *fascia cruris* (of the calf) and then separate IMAT and muscle tissue within the fascia. In this case segmentation of individual muscles is not performed. Segmentation of individual muscles is usually required for NMD as muscles are affected differently by the disease [4,130,131].

One example workflow is outlined in Fig. 3. The T1w dataset is used for an automatic segmentation of the fascia lata. The segmentation map is then transferred by 3D co-registration to a Dixon fat fraction map where segmentation of IMAT and muscle tissue is performed (Fig. 4). Finally, T2 water results are obtained in muscle tissue using a T2 map (Fig. 3 right) 3D registered to the Dixon fat fraction map. This workflow demonstrates a number of important requirements of advanced MR muscle analysis. First, the combination of multiple MR sequences, which typically have different spatial resolutions and which may also be affected by subject motion between acquisitions requires sophisticated 3D registration algorithms. Second, a differentiation of SAT and IMAT, which was not performed in earlier studies of the thigh [132] requires a segmentation of the fascia lata, which is hardly visible in Dixon images. Thus T1w may be preferable for the segmentation of the fascia lata although it is still difficult to track in T1w images. In younger subjects (Fig. 2a) a tight muscle envelope, which is relatively easy to segment [133–136], can be used as substitute of the fascia lata. However, in elderly subjects the fascia lata is no longer in overall contact with muscle but locally separated by layers of adipose tissue (Fig. 5). Recently advanced semi-automatic [137,138] as well as deep learning based [139,140] fascia segmentation procedures with good accuracy and precision have been developed but current deep learning models are based on rather small amounts of training and validation data. Thus they are still very specialized and further validation of more general models is needed.

In a second workflow shown in Fig. 6 individual muscles are manually segmented in the T1w images and segmentation masks are 3D registered to Dixon maps. In the Dixon image a PDFF threshold is applied to differentiate muscle and adipose tissue of each segmented muscle. Obviously the manual segmentation of multiple slices is challenging but high agreement among experts with ICC values of >0.94 in the thigh [141–143] and of >0.98 in the spine [144] have been reported. An excellent review of segmentation of individual muscle has recently been published [128]. So far in NMD, the performance of automated segmentation techniques was poor because of varying degrees of replacement of muscle by adipose tissue. However, recently accurate results with Dice ratios of around 0.9 when comparing of automated and manual segmentation results have been reported [138,139,145,146].

A third workflow (Fig. 7) shows the segmentation of paraspinal muscles, left and right psoas and erector spinae muscles of the lumbar spine. In some publications multifidus, longissimus and ilocostalis lumborum of the erector spinae are further differentiated [147–149] and the quadratus lumborum has also been analyzed [150,151]. Depending on available data and parameters to be quantified other workflows may be preferable to the ones discussed above.

5.2. Quantitative measurements

Table 2 lists common parameters to quantify muscle properties with MRI or MRS. Muscle area/volume can be obtained directly from T1 weighted images, which provide good spatial resolution but are often affected by inhomogeneity artifacts, which as shown in Fig. 3 may still persist after bias correction using N3 or N4 algorithms [152]. Also T1w grey values are not standardized or normalized, which complicates any threshold based segmentation. A large variety of methods to determine muscle area/volume have been published [153]. For comparability absolute measurements such as volume or area should be normalized, for example to body height or in the thigh to the leg volume/diameter. IMAT and muscle tissue volume could also be normalized to the fascia volume [154]. PDFF, $T2_w$, $T2_f$, and TSC values are measured directly in the corresponding images as mean intensity values, however, as outlined in the preceding sections, these sequences require dedicated signal reconstruction or post processing to generate the specific parameter maps.

For the differentiation between adipose and muscle components a threshold applied to a Dixon PDFF map and sometimes even to T1w images has been used. For example, a 50% PDFF threshold [155,156] has been suggested but in healthy and even sarcopenic subjects this seems high as muscle tissue PDFF is below 20%. One level of sophistication is the use of subject adaptive thresholds obtained from a histogram analysis [137,157,158] but different threshold techniques may result in large differences in IMAT volume [159]. Other authors have developed k-means clustering [160] or fuzzy c-means algorithms [161] to differentiate IMAT and muscle tissue. A comparison of more advanced methods such as level sets, Gaussian mixture models, graph cuts and shape prior level sets showed that the choice of the best method depended on the severity of fat infiltration [162].

It is important to note that analysis results depend on spatial resolution as shown for IMAT and muscle tissue in Fig. 4. In vivo imaging is always affected by partial volume artefacts caused by small agglomerations of adipocytes. Thus PDFF of those muscle tissue voxel located at the border with IMAT will be too high and a peeling operation of the muscle tissue VOI before calculation of PDFF may be indicated but here further research and standardization is required.

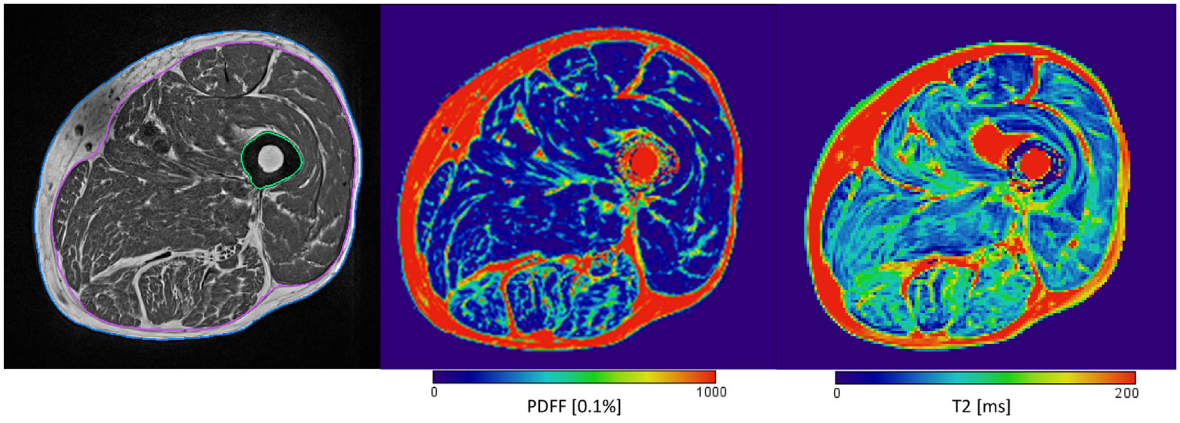

Fig. 3. Left: T1 weighted sequence after bias correction, with segmented fascia lata (pink); center Dixon fat fraction map after 3D registration to T1w sequence and registration of fascia lata. Right: T2 map after registration to Dixon sequence. One axial slice of 3D dataset shown each. Bias correction did not remove all artifacts in the T1w image.

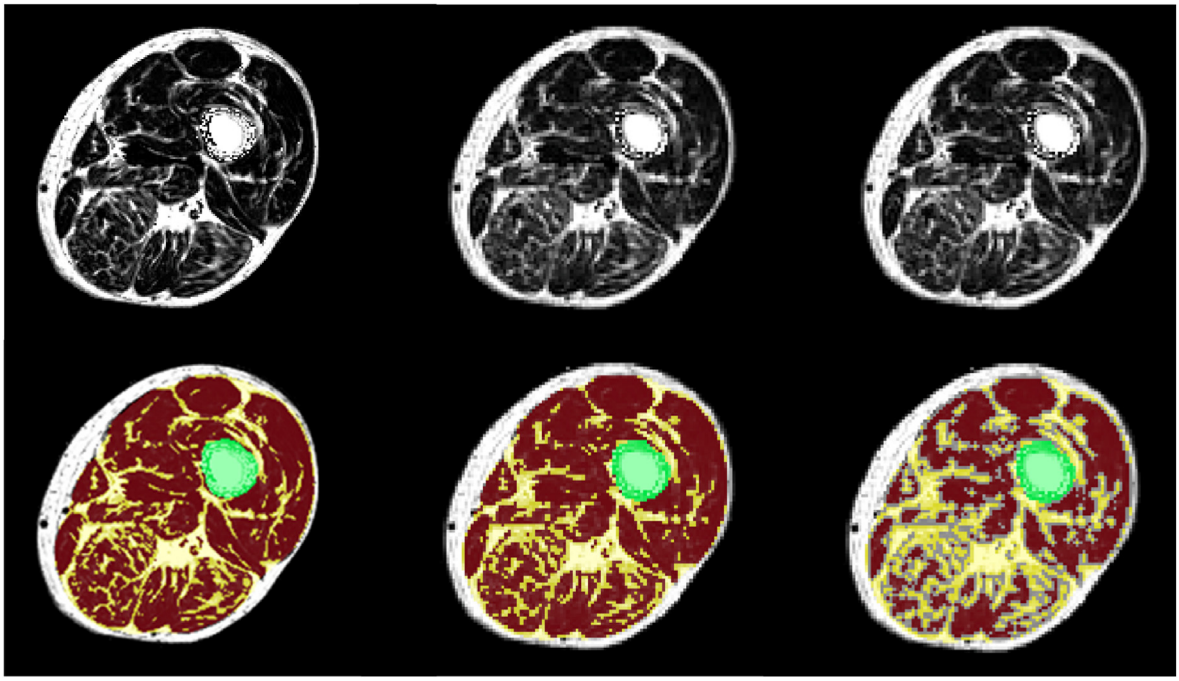

Fig. 4. Dixon fat fraction map without (top) and with (bottom) segmentation of IMAT and muscle tissue. Left: high resolution (in plane pixel size x slice thickness - 0.98 × 0.98 × 3.0 mm^3); center: standard resolution (1.56 × 1.56 × 3.0 mm^3); right: same resolution as center but muscle tissue peeled by one voxel. The figure shows one slice out of 29 of the acquired 3D dataset. Results of the complete dataset for muscle tissue (MT) volume and proton density fat fraction (PDFF) depend on spatial resolution and on segmentation technique. Left: MT vol = 985 cm^3, PDFF = 8.7%; center: MT vol = 923 cm^3, PDFF = 13.2%; right: MT vol = 500 cm^3, PDFF = 10.2%.

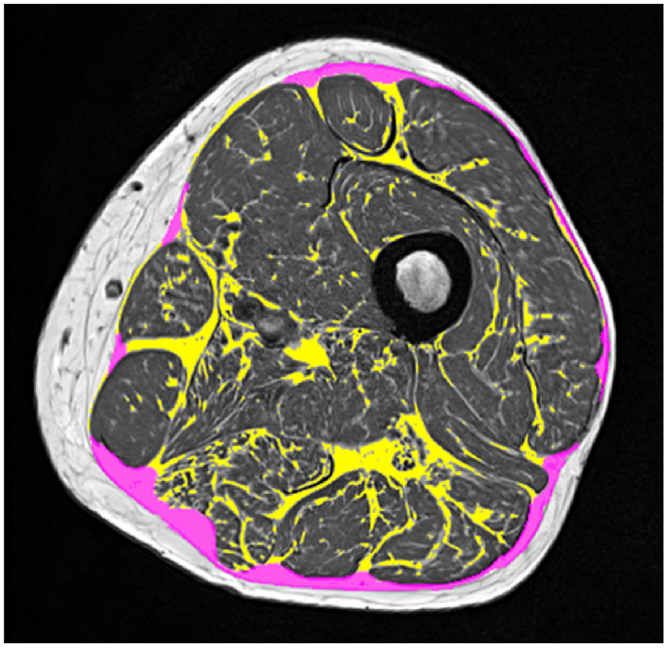

Fig. 5. In elderly subjects the fascia lata is not always in direct contact with muscle but partly separated by layers of adipose tissue (pink), which are part of intermuscular adipose tissue (IMAT). A tight muscle envelope excluding most or all of the pink ROI would significantly decrease the volume of IMAT (yellow). In younger subjects Fig. 2a there is no or very little adipose tissue located between muscle and fascia. (For interpretation of the references to color in this figure legend, the reader is referred to the Web version of this article.)

6. Muscle imaging in clinical trials

Muscle MRI has been increasingly used for quantification of muscle properties in longitudinal studies to evaluate efficacy of therapeutic interventions or to document disease effects over time [163–170] Only a few multicenter trials have been published [171–176]. Outcome of clinical trials is typically the comparison of percentage change over time between a treated and a control group for a given quantitative parameter such as PDFF. Minimization of longitudinal precision errors is of high importance. Low accuracy errors are important to compare assessments across scanners but as long as accuracy errors do not change longitudinally their impact on a clinical trial endpoint is less relevant. Precision errors for parameters listed in Table 2 are summarized in Table 3.

In designing multicenter trials special challenges must be considered so that imaging is performed in a consistent manner when utilizing scanners from different manufacturers with different field strength. The design of MRI subject positioning procedures, sequence parameters, and data analyses must be standardized to ensure that imprecision does not mask the expected physiological change.

Change in muscle tissue volume over time specifically in the thigh has been the main MRI based biomarker used in single- and multicenter trials. MRI data acquisition for this task can be easily standardized across multiple sites as it does not require advanced sequences or modern hardware. Spin echo-based sequences should be used either for a set number of slices acquired at the center of the muscle or for the entire length of the muscle bundle. Spin echo sequences are superior to Gradient recalled echo sequences in producing sharper images, because they are less sensitive to susceptibility artifacts that can arise from fatty inflation [185]. Axial images with an in-plane resolution close to 1 mm and 5–8 mm slice thickness in the thighs have been used [186], as compared to approximately 0.5–0.75 mm and 2–4 mm slices in the arms and calves [187].

Fat fraction is another biomarker that has been implemented in multicenter trials. 2 pt Dixon based approaches are widely available but not all sites participating in a multi center trial may have used them in clinical routine. Sometimes the Dixon sequence still must be set up on a scanner, which typically requires tuning and optimization. Dedicated training of the technicians performing the muscle scans may also be required Three or more echoes have been used [60] but these sequences

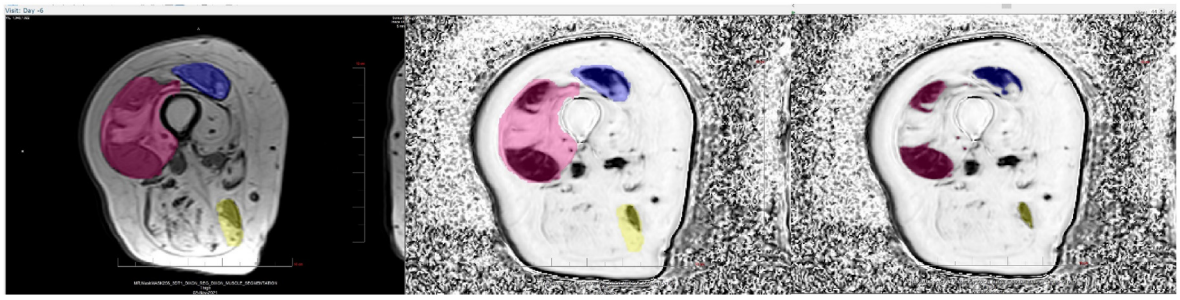

Fig. 6. Left: Manual contouring of individual muscles (here: vastus medialis, rectus femoris and biceps femoris) in T1 weighted sequence; center Dixon FF map after 3D registration to T1w sequence and registration of muscle contours. Right: Threshold based separation of muscle tissue and adipose tissue compartments of each segmented muscle.

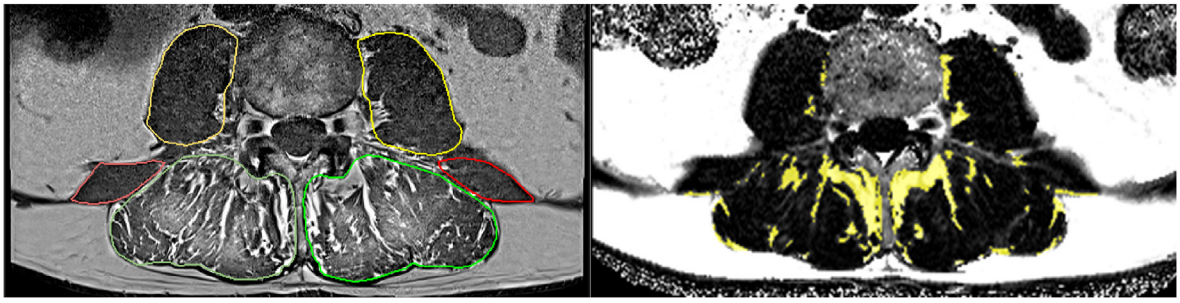

Fig. 7. Segmentation and analysis of paraspinal muscles of the lumbar spine. Left. T1w images with segmented psoas, erector spinae and quadratus lumborum muscles; right: Dixon FF map 3D registered to T1w sequence and registered segmentation maps.

Table 2
Determination of common quantitative muscle parameters by technique. ADC: apparent diffusion coefficient; DTI: diffusion tensor imaging; EMCL: extramyocellular lipids; FA: fractional anisotropy; IMAT: intermuscular adipose tissue; IMCL intramyocellular lipids; MRS: magnetic resonance spectroscopy; PDFF: proton density fat fraction; $T2_w$: T2 water [ms]; $T2_w$: T2 fat [ms]; *DTI based tractography.

Parameter	T1w	Dixon FF	T2 map	DTI	MRS
SAT area/volume (cm^2/cm^3)	++	+	+/−	—	
muscle area/volume (cm^2/cm^3)	++	+	+/−	—	
IMAT area/volume (cm^2/cm^3)	+	++	+/−	—	
muscle tissue area/volume (cm^2/cm^3)	+	++	+/−	—	
intra fascia PDFF (%)	—	++	—	—	
muscle tissue PDFF (%)	—	++	—	—	+
$T2_w$ (ms)	—	—	++	—	
$T2_f$ (ms)	—	—	++	—	
EMCL (mmol/kg)	—	—	—	—	++
IMCT (mmol/kg)	—	—	—	—	++
ADC, FA				++	
pennation angle, curvature, fiber length, and physiological cross-sectional area				++*	

are not as widely available as 2 pt Dixon sequences. For a multi-center trial the scan of a phantoms to evaluate the accuracy of the fat fraction maps and to determine if water/fat swap artifacts occur is recommended [178]. A simple fat and water phantom suffices to configure the sequence but phantoms with a larger range of fat fractions such as the PDFF phantom from Calimetrix (Calimetrix, Inc, Madison, WI, USA) could be useful (Fig. 8). In a recent multicenter study with different scanner types initiated by the PDFF Biomarker Committee within the Quantitative Imaging Biomarkers Alliance (QIBA) of the Radiological Society of North America, PDFF accuracy errors were below 5% [188].

T2 mapping is even more challenging to implement in multicenter trials due to the variability in the implementation of the MSE sequences among different manufactures. On many scanners the number of echos is limited preventing the fit of multi exponential fits (see section on T2 maps). Thus $T2_w$ and $T2_f$ cannot be differentiated. As a consequence, fat suppressed T2 sequences must be used. However, fat suppression is usually not perfect and accuracy of $T2_w$ is lower than with non-fat suppressed T2 sequences. For these around 20 echos are required, which is only feasible with modern scanners.

7. Future directions

Quantitative MR imaging techniques have significantly matured during the last decade, however, assessments must be better standardized. Even the terminology with respect to IMAT is not unequivocal. The clinical interpretation of outcome parameters is not always obvious and small differences in segmentation algorithms may have a significant impact on numerical results. There is a lack of data on accuracy and precision. Given the large variety of MR sequences and implementation differences between manufacturers, standardization of accuracy measurements is of high importance. One potential avenue is the use of phantoms, as demonstrated in a recent PDFF study [188] but these efforts must be extended to all the techniques described above. Also, mid- and long-term stability of phantoms, which often contain fluids, is still questionable.

Further, gender and ethic specific normal data such age-related changes of quantitative outcome parameters are required for putting intervention effects into perspective. Very little data have been published [189–194] so far. Published data on precision, which are summarized in Table 3 are encouraging but it remains to be shown whether these data typically obtained in very experienced research centers can be achieved in clinical routine or in multicenter trials. Currently, multicenter trials with quantitative endpoints are rather difficult to conduct in particular if scanners from different manufactures or even of different makes from a given manufacturer are used. Missing standardization of installed MR sequences and available coils further complicates and increases cost of such trials.

Table 3
Precision errors of quantitative parameters shown in Table 2. The time period between repeated measurements is indicated in column 'Period'. ST: short term (same day); the digit after ST denotes the number of total acquisitions;/repos: subjects were repositioned between acquisitions. Depending on publication, precision errors are either reported as root mean square coefficient of variation (CV_{RMS}) in % [177] or as intraclass correlation coefficients (ICC). IF: intra fascia; PDFF: proton density fat fraction; wb: whole body.

ref	parameter	Anatomy	technique	population	Period	Statistics	Value
[178]	SAT volume	abdomen	2 pt wb Dixon	18 subjects ♂ & ♀ age range 24–51	ST 2 5 different scanners	%CV	4.4
[179]	IF muscle area muscle area	thigh hip adductor hip flexor	T1w	14 subjects ♂ & ♀ age range 21–68	ST 3	$\%CV_{RMS}$	1.3 1.6 1.8
[178]	muscle volume	total thigh	2 pt wb Dixon	18 subjects ♂ & ♀ age range 24–51	ST 2 5 different scanners	%CV	0.87
[180]	muscle tissue volume	thigh adductors quadriceps spinus erectae	2 pt wb Dixon	16 subjects ♂ & ♀ age range 23–65	4–12 weeks	%CV	3.4 3.5 7.0
[181]	muscle tissue volume	thigh	T1w	20 subjects ♂ & ♀ age range 25–76	ST 2/repos	ICC	0.996
[182]	muscle tissue volume	thigh	6 pt Dixon	23 young healthy ♂ 24 elderly sarcopenic ♂	ST 2/repos	$\%CV_{RMS}$	1.2 1.5
[178]	muscle fat infiltration	anterior/posterior lef/right thigh	2 pt wb Dixon	18 subjects ♂ & ♀ age range 24–51	ST 2 5 different scanners	%CV	10.8–14.4%
[182]	IF PDFF	thigh	6 pt Dixon	23 young healthy ♂ 24 elderly sarcopenic ♂	ST 2/repos	$\%CV_{RMS}$	2.1 1.6
[183]	IF PDFF	thigh	4 pt Dixon	65 young healthy ♂ & ♀	ST 3	ICC	0.999
[184]	IF PDFF	thigh calf	3 pt Dixon	14 young healthy ♂ & ♀	2 weeks	ICC	0.91 0.89
[182]	muscle tissue PDFF	thigh	MRS	23 young healthy ♂ 24 elderly sarcopenic ♂	ST/repos	$\%CV_{RMS}$	15.3 9.0
[183]	$T2_w$	thigh	T2/17 echos	65 young healthy ♂ & ♀	ST	ICC	0.986
[183]	ADC	thigh	DTI	65 young healthy ♂ & ♀	ST	ICC	0.963

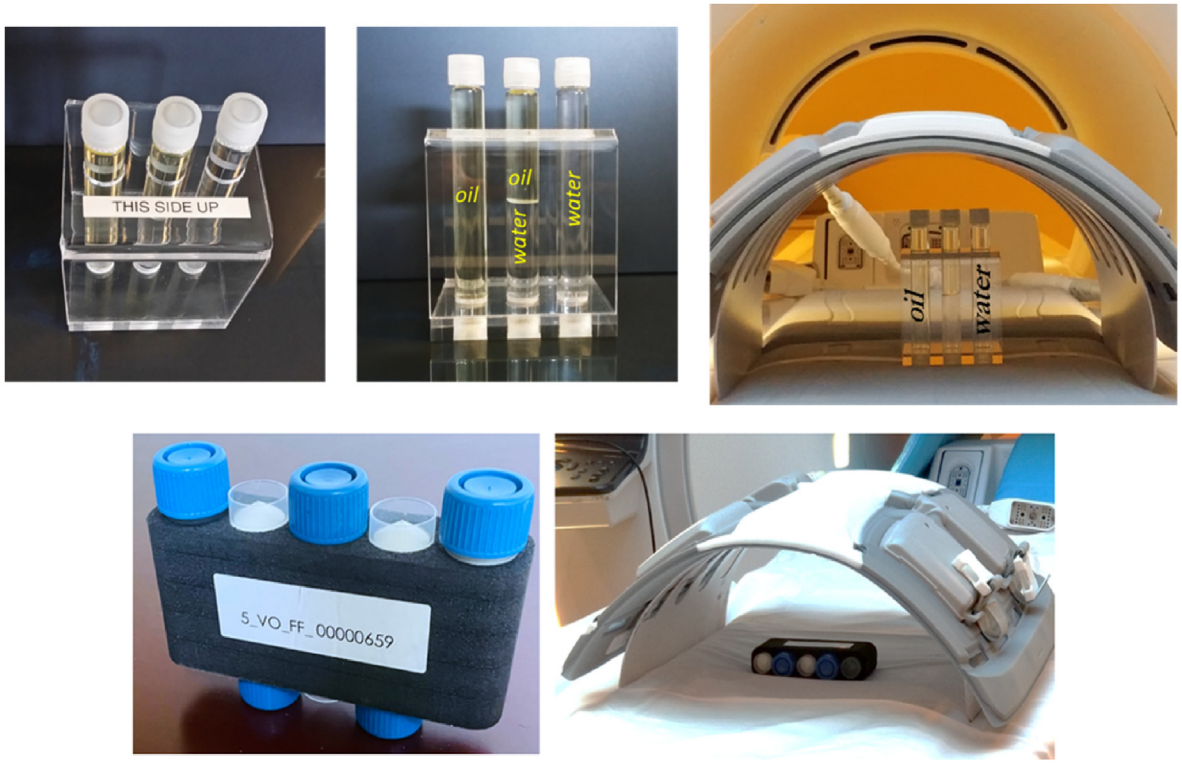

Fig. 8. Phantoms for calibration of Dixon sequences. Top: Clario FF phantom with pure water and fat inserts; bottom: Calimetrix PDFF phantom with 5 inserts containing 0, 10, 20, 30, and 40% fat fraction.

It is a promise to clinicians that via the use of quantitative MRI using PDFF and $T2_w$ maps muscle disease can be diagnosed earlier than with standard techniques. PDFF and $T2_w$ are related to inflammatory processes preceding muscle fat infiltration and destruction. DTI and perhaps ^{23}Na MRI, which probe pathophysiological changes at the cellular or fascicular level, hold some promise to allow for diagnosis at even earlier stages of the disease and eventually may allow for design of personalized interventions. The use of multiple MRI scans such as T1w, Dixon and T2 maps has been reported in many studies but overall scan time should be shortened, sequences should have similar spatial resolution and a

common reference system so that they can easily be registered together.

The association of quantitative MRI parameters with muscle function warrants further investigations. In NMD, for example many cross-sectional studies have demonstrated clinically relevant correlations between MRI and muscle function but only a few studies have presented longitudinal results [130]. Even less is known on how age or for example exercise related changes of MRI parameters can predict direct changes in muscle strength. In normal or sarcopenic subjects muscle strength can be rapidly increased by about 30% through exercise. Thus exercise is an important intervention for sarcopenia but its pathophysiological effect on muscle is still difficult to evaluate. First studies have shown the potential of DTI based fiber tractography.

In summary, quantitative MRI provides new avenues for significant advances in muscle research using in vivo imaging but standardization of almost all of its procedures combined with a tighter integration of the analysis into the workflow will be key to its more widespread clinical use.

Author contributions

Each author contributed manuscript text according to his or her specific expertise. KE assembled all text blocks into the final manuscript, which was reviewed, edited and approved by all coauthors.

Funding

There was no specific funding available for this study.

Declaration of competing interest

The authors declare that the research was conducted in the absence of any commercial or financial relationships that could be construed as a potential conflict of interest. KE is a part time and MABE a full time employee of Clario, Inc.

15 Technical Appendix

15.1 Dixon Imaging

In 1984, Dixon introduced a 'simple proton spectroscopic imaging' technique [195], which decomposes fat and water components of the proton signal into two separate image maps by exploiting the difference in resonance frequencies between fat and water protons (chemical shift). Dixon showed that there is an oscillation of the free induction decay (FID) of the magnetization of a voxel containing fat and water after a 90° pulse. At the start (t = 0) of the free induction decay the magnetization vectors of water and fat point in the same direction (IP: in phase. The first minimum of the FID occurs at t_{min1}

$$t_{min\ 1} = \frac{1}{2(\nu_w - \nu_f)}$$

at t_{min1} magnetization vectors of water and fat point in opposite direction (OP: opposed phase). ν_w and ν_f are the Lamor frequencies of water and fat, respectively. The chemical shift between water and fat is ≈ 3.4 ppm which translates into $\Delta\nu = \nu_w - \nu_f \approx 220$ Hz at 1.5 T and $\Delta\nu \approx 440$ Hz at 3 T.

In theory the sum of IP and OP images divided by 2 results in a so-called water image and the difference divided by 2 in a so-called fat image. Fat fraction (FF) and water fraction (WF) images can then be calculated as:

FF = fat image/ (fat image + water image)

WF = water image / (fat image + water image)

In reality, fat quantification accuracy of the simple IP-OP approach is impaired by magnetic field inhomogeneities, T2*-decay, T_1-bias, spectral complexity of fat, noise bias and eddy currents [164,196–200]. Magnetic field inhomogeneities for example increase the probability of wrong phase assignments which cause local fat-water swaps [201–203]. These limitations have triggered significant improvements of the original 2 pt Dixon technique incorporating more sophisticated signal models such as the use of flexible echo times [61,197,204,205] and the introduction of 3 pt or 6 pt echo techniques [206–210]. With these advanced Dixon techniques exact IP and OP imaging is no longer required [211–213]. Another area of improvement is signal processing. For example, the T2* decay caused by increasing echo times after RF excitation can be corrected by incorporation of T2* into the signal model used to calculate the fat fraction [214–218].

15.2 T2 maps

Multi-exponential T2 fitting [73] exploits the strong differences in relaxation times between water and fat. The total signal decay is modeled as a combination of the individual water and fat signals, weighted by the respective volume fractions. The fat signal is further assumed to consist of multiple components possessing different relaxation properties. For example, a tri-exponential T2 model (Figure-A 1) assumes two dominant fat components, one possessing a shorter relaxation time ($T2_{s,fat}$) and a signal fraction of $f_{s,fat}$ possessing a longer relaxation time ($T2_{l,fat}$) and a contribution of (1-$f_{s,fat}$). The total resulting signal is therefore [73]:

$$S = S_f\left(f_{s,fat}\ \exp\left(-\frac{TE}{T2_{s,fat}}\right) + (1-f_{s,fat})\exp\left(-\frac{TE}{T2_{l,fat}}\right)\right) + S_w\ \exp\left(-\frac{TE}{T2_{water}}\right).$$

here, S_f and S_w describe the overall signal intensities of fat and water, respectively. As this model requires the determination of several fit parameters, it is unstable if only a limited number of echoes are acquired. Therefore, relaxation parameters of adipose tissue are usually determined first, e.g. within subcutaneous fat or bone marrow, and then fixed in the tri-exponential model to enhance fit stability [73]. However, multi-exponential fitting models generally do not consider inhomogeneities in the B1 field as well as stimulated echoes [219], which can influence the resulting T2 values.

To overcome these limitations, T2 fitting exploiting extended phase graphs (EPG) has been proposed [220]. Using the EPG approach, the signal evolution is simulated for various combinations of T2 as well as relative B1 and FF values. Then, a mapping of the measured signal decay to the

simulated curves is performed to find the corresponding parameters for each voxel [220,221]. By including B1 in the simulation, EPG approaches offer higher stability with respect to an inhomogeneous transmit field, and correct for stimulated echoes. Recent implementations of EPG T2 fitting also consider the slice flip angle profiles and chemical shift displacement in slice direction, enabling a reliable T2 determination even in case of large FF > 50% [222].

15.3 Diffusion tensor imaging

Diffusion tensor imaging (DTI) [77] is a technique to determine a map of the six components of the diffusion tensor D with its eigenvalues λ_1, λ_2 and λ_3 [223]. The magnitude of the eigenvectors characterizes the degree of anisotropy of the diffusion, which in the axial muscle fiber direction (λ_1) is higher than in the radial fiber direction (λ_2 and λ_3). Further outcomes of DTI are MD also termed apparent diffusion coefficient (ADC) and the fractional anisotropy FA as given by the formulas below

$$D = \begin{Bmatrix} D_{xx} & D_{xy} & D_{xz} \\ D_{yx} & D_{yy} & D_{yz} \\ D_{zx} & D_{zy} & D_{zz} \end{Bmatrix} \quad \text{with } D_{xy} = D_{yx};\ D_{xz} = D_{zx};\ D_{yz} = D_{zy}$$

$$MD = ADC = \frac{\lambda_1 + \lambda_2 + \lambda_3}{3} = \bar{\lambda}$$

$$FA = \sqrt{\frac{2}{3}} \cdot \sqrt{\left(\frac{(\lambda_1 - \bar{\lambda})^2 + (\lambda_2 - \bar{\lambda})^2 + (\lambda_3 - \bar{\lambda})^2}{\lambda_1^2 + \lambda_2^2 + \lambda_3^2} \right)}$$

15.4 Appendix - Figures

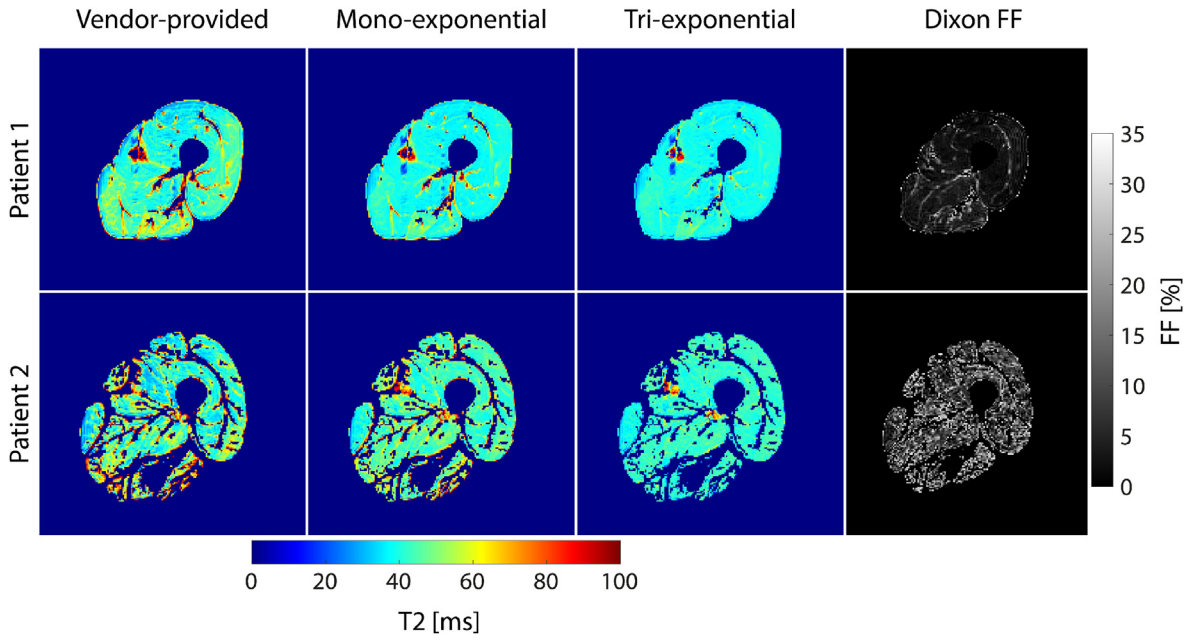

Fig. A1. T2 maps and corresponding Dixon FF maps of a subject with lower and a subject with higher muscle tissue FF (patient 1, mean FF = 4.9%; patient 2, mean FF = 13.1%). In subject 2 with higher FF, T2 values are elevated, particularly in the vendor-provided T2 map, but also in the mono-exponentially fitted T2 map. In contrast, T2 values were similar for both patients in the tri-exponential T2 map. Moreover, within the thigh muscle of subject 1, a variation could be observed between individual muscles in the product T2 map, which was not present in the custom-fit T2 maps.

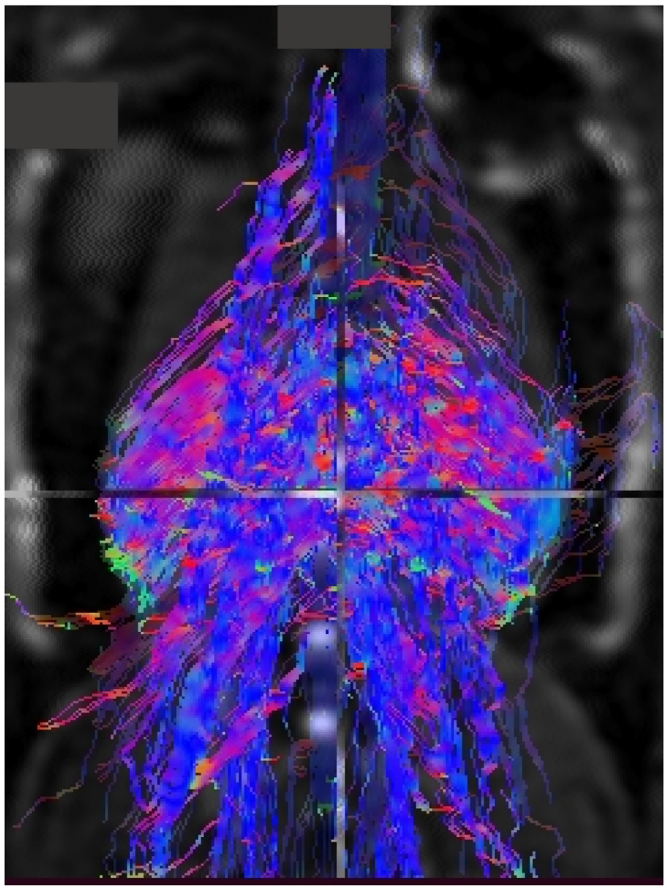

Fig. A2. Illustration of paraspinal muscle fibers of a rat using tractography.

References

[1] Mercuri E, Pichiecchio A, Allsop J, Messina S, Pane M, Muntoni F. Muscle MRI in inherited neuromuscular disorders: past, present, and future. J Magn Reson Imag 2007 Feb;25(2):433–40.

[2] Paoletti M, Pichiecchio A, Cotti Piccinelli S, Tasca G, Berardinelli AL, Padovani A, et al. Advances in quantitative imaging of genetic and acquired myopathies: clinical applications and perspectives. Front Neurol 2019;10:78.

[3] Smitaman E, Flores DV, Mejia Gomez C, Pathria MN. MR imaging of atraumatic muscle disorders. Radiographics 2018 Mar-Apr;38(2):500–22.

[4] Ten Dam L, van der Kooi AJ, Verhamme C, Wattjes MP, de Visser M. Muscle imaging in inherited and acquired muscle diseases. Eur J Neurol 2016 Apr;23(4): 688–703.

[5] Weber A, editor. Magnetic resonance imaging of skeletal musculature. Heidelberg: Springer; 2014.

[6] Mercuri E, Pichiecchio A, Counsell S, Allsop J, Cini C, Jungbluth H, et al. A short protocol for muscle MRI in children with muscular dystrophies. Eur J Paediatr Neurol : EJPN : official journal of the European Paediatric Neurology Society 2002;6(6):305–7.

[7] Mercuri E, Talim B, Moghadaszadeh B, Petit N, Brockington M, Counsell S, et al. Clinical and imaging findings in six cases of congenital muscular dystrophy with rigid spine syndrome linked to chromosome 1p (RSMD1). Neuromuscul Disord : NMD 2002 Oct;12(7–8):631–8.

[8] Jungbluth H, Sewry CA, Counsell S, Allsop J, Chattopadhyay A, Mercuri E, et al. Magnetic resonance imaging of muscle in nemaline myopathy. Neuromuscul Disord : NMD 2004 Dec;14(12):779–84.

[9] Lamminen AE. Magnetic resonance imaging of primary skeletal muscle diseases: patterns of distribution and severity of involvement. Br J Radiol 1990 Dec; 63(756):946–50.

[10] Goutallier D, Postel JM, Bernageau J, Lavau L, Voisin MC. Fatty muscle degeneration in cuff ruptures. Pre- and postoperative evaluation by CT scan. Clin Orthop Relat Res 1994 Jul;(304):78–83.

[11] Goutallier D, Postel JM, Bernageau J, Lavau L, Voisin MC. Fatty infiltration of disrupted rotator cuff muscles. Rev Rhum Engl Ed 1995 Jun;62(6):415–22.

[12] Poliachik SL, Friedman SD, Carter GT, Parnell SE, Shaw DW. Skeletal muscle edema in muscular dystrophy: clinical and diagnostic implications. Phys Med Reh Clin N 2012 Feb;23(1):107–+.

[13] Lamminen AE, Tanttu JI, Sepponen RE, Suramo IJ, Pihko H. Magnetic resonance of diseased skeletal muscle: combined T1 measurement and chemical shift imaging. Br J Radiol 1990 Aug;63(752):591–6.

[14] Lamminen AE, Tanttu JI, Sepponen RE, Pihko H, Korhola OA. T1 rho dispersion imaging of diseased muscle tissue. Br J Radiol 1993 Sep;66(789):783–7.

[15] Hollingsworth KG, de Sousa PL, Straub V, Carlier PG. Towards harmonization of protocols for MRI outcome measures in skeletal muscle studies: consensus recommendations from two TREAT-NMD NMR workshops, 2 May 2010, Stockholm, Sweden, 1-2 October 2009, Paris, France. Neuromuscul Disord : NMD 2012 Oct 1;22(Suppl 2):S54–67.

[16] Strijkers GJ, Araujo ECA, Azzabou N, Bendahan D, Blamire A, Burakiewicz J, et al. Exploration of new contrasts, targets, and MR imaging and spectroscopy techniques for neuromuscular disease - a workshop report of working group 3 of the biomedicine and molecular biosciences COST action BM1304 MYO-MRI. J Neuromuscul Dis 2019;6(1):1–30.

[17] Cohen S, Nathan JA, Goldberg AL. Muscle wasting in disease: molecular mechanisms and promising therapies. Nat Rev Drug Discov 2015 Jan;14(1): 58–74.

[18] Arbanas J, Pavlovic I, Marijancic V, Vlahovic H, Starcevic-Klasan G, Peharec S, et al. MRI features of the psoas major muscle in patients with low back pain. Eur Spine J 2013 Sep;22(9):1965–71.

[19] Paalanne N, Niinimaki J, Karppinen J, Taimela S, Mutanen P, Takatalo J, et al. Assessment of association between low back pain and paraspinal muscle atrophy using opposed-phase magnetic resonance imaging: a population-based study among young adults. Spine (Phila Pa 1976) 2011 Nov 1;36(23):1961–8.

[20] Sollmann N, Bonnheim NB, Joseph GB, Chachad R, Zhou J, Akkaya Z, et al. Paraspinal muscle in chronic low back pain: comparison between standard parameters and chemical shift encoding-based water-fat MRI. J Magn Reson Imag 2022 Mar 14.

[21] Yanik B, Keyik B, Conkbayir I. Fatty degeneration of multifidus muscle in patients with chronic low back pain and in asymptomatic volunteers: quantification with chemical shift magnetic resonance imaging. Skeletal Radiol 2013 Jun;42(6): 771–8.

[22] Ahn H, Kim DW, Ko Y, Ha J, Shin YB, Lee J, et al. Updated systematic review and meta-analysis on diagnostic issues and the prognostic impact of myosteatosis: a new paradigm beyond sarcopenia. Ageing Res Rev 2021 Sep;70:101398.
[23] Sergi G, Trevisan C, Veronese N, Lucato P, Manzato E. Imaging of sarcopenia. Eur J Radiol 2016 Aug;85(8):1519–24.
[24] Boutin RD, Yao L, Canter RJ, Lenchik L. Sarcopenia: current concepts and imaging implications. AJR Am J Roentgenol 2015 Sep;205(3):W255–66.
[25] Addison O, Drummond MJ, LaStayo PC, Dibble LE, Wende AR, McClain DA, et al. Intramuscular fat and inflammation differ in older adults: the impact of frailty and inactivity. J Nutr Health Aging 2014 May;18(5):532–8.
[26] Herrmann M, Engelke K, Ebert R, Muller-Deubert S, Rudert M, Ziouti F, et al. Interactions between muscle and bone-where physics meets biology. Biomolecules 2020 Mar 10;10(3).
[27] Chi AS, Long SS, Zoga AC, Parker L, Morrison WB. Association of gluteus medius and minimus muscle atrophy and fall-related hip fracture in older individuals using computed tomography. J Comput Assist Tomogr 2016 Mar-Apr;40(2):238–42.
[28] Lang T, Cauley JA, Tylavsky F, Bauer D, Cummings S, Harris TB, et al. Computed tomographic measurements of thigh muscle cross-sectional area and attenuation coefficient predict hip fracture: the health, aging, and body composition study. J Bone Miner Res 2010 Mar;25(3):513–9.
[29] Lang T, Koyama A, Li C, Li J, Lu Y, Saeed I, et al. Pelvic body composition measurements by quantitative computed tomography: association with recent hip fracture. Bone 2008 Apr;42(4):798–805.
[30] Muhlberg A, Museyko O, Bousson V, Pottecher P, Laredo JD, Engelke K. Three-dimensional distribution of muscle and adipose tissue of the thigh at CT: association with acute hip fracture. Radiology 2019 Feb;290(2):426–34.
[31] Wang L, Yin L, Yang M, Ge Y, Liu Y, Su Y, et al. Muscle density is an independent risk factor of second hip fracture: a prospective cohort study. J Cachexia Sarcopenia Muscle 2022 Jun;13(3):1927–37.
[32] Daguet E, Jolivet E, Bousson V, Boutron C, Dahmen N, Bergot C, et al. Fat content of hip muscles: an anteroposterior gradient. J Bone Joint Surg Am 2011 Oct 19;93(20):1897–905.
[33] Engelke K, Museyko O, Wang L, Laredo JD. Quantitative analysis of skeletal muscle by computed tomography imaging-State of the art. J Orthop Translat 2018 Oct;15:91–103.
[34] Karampinos DC, Baum T, Nardo L, Alizai H, Yu H, Carballido-Gamio J, et al. Characterization of the regional distribution of skeletal muscle adipose tissue in type 2 diabetes using chemical shift-based water/fat separation. J Magn Reson Imag 2012 Apr;35(4):899–907.
[35] Correa-de-Araujo R, Addison O, Miljkovic I, Goodpaster BH, Bergman BC, Clark RV, et al. Myosteatosis in the context of skeletal muscle function deficit: an interdisciplinary workshop at the national Institute on aging. Front Physiol 2020;11:963.
[36] Boesch C. Musculoskeletal spectroscopy. J Magn Reson Imag 2007 Feb;25(2):321–38.
[37] Barker AR, Armstrong N. Insights into developmental muscle metabolism through the use of 31P-magnetic resonance spectroscopy: a review. Pediatr Exerc Sci 2010 Aug;22(3):350–68.
[38] Deshmukh S, Subhawong T, Carrino JA, Fayad L. Role of MR spectroscopy in musculoskeletal imaging. Indian J Radiol Imag 2014 Jul;24(3):210–6.
[39] Meyerspeer M, Boesch C, Cameron D, Dezortova M, Forbes SC, Heerschap A, et al. 31) P magnetic resonance spectroscopy in skeletal muscle: experts' consensus recommendations. NMR Biomed 2020 Feb 10:e4246.
[40] Harris RK, Becker ED, De Menezes SMC, Goodfellow R, Granger P. NMR nomenclature. Nuclear spin properties and conventions for chemical shifts - (IUPAC recommendations 2001). Pure Appl Chem 2001 Nov;73(11):1795–818.
[41] Pola A, Sadananthan SA, Yaligar J, Nagarajan V, Han W, Kuchel PW, et al. Skeletal muscle lipid metabolism studied by advanced magnetic resonance spectroscopy. Prog Nucl Magn Reson Spectrosc 2012 Aug;65:66–76.
[42] Boesch C, Slotboom J, Hoppeler H, Kreis R. In vivo determination of intra-myocellular lipids in human muscle by means of localized 1H-MR-spectroscopy. Magn Reson Med 1997 Apr;37(4):484–93.
[43] Krssak M, Lindeboom L, Schrauwen-Hinderling V, Szczepaniak LS, Derave W, Lundbom J, et al. Proton magnetic resonance spectroscopy in skeletal muscle: experts' consensus recommendations. NMR Biomed 2021 May;34(5):e4266.
[44] Alhulail AA, Patterson DA, Xia P, Zhou X, Lin C, Thomas MA, et al. Fat-water separation by fast metabolite cycling magnetic resonance spectroscopic imaging at 3 T: A method to generate separate quantitative distribution maps of musculoskeletal lipid components. Magn Reson Med 2020 Sep;84(3):1126–39.
[45] Nagarajan R, Carpenter CL, Lee CC, Michael N, Sarma MK, Souza R, et al. Assessment of lipid and metabolite changes in obese calf muscle using multi-echo echo-planar correlated spectroscopic imaging. Sci Rep 2017 Dec 11;7(1):17338.
[46] Vermathen P, Kreis R, Boesch C. Distribution of intramyocellular lipids in human calf muscles as determined by MR spectroscopic imaging. Magn Reson Med 2004 Feb;51(2):253–62.
[47] Kim HK, Serai S, Lindquist D, Merrow AC, Horn PS, Kim DH, et al. Quantitative skeletal muscle MRI: Part 2, MR spectroscopy and T2 relaxation time mapping-comparison between boys with duchenne muscular dystrophy and healthy boys. AJR Am J Roentgenol 2015 Aug;205(2):W216–23.
[48] Barnard AM, Willcocks RJ, Finanger EL, Daniels MJ, Triplett WT, Rooney WD, et al. Skeletal muscle magnetic resonance biomarkers correlate with function and sentinel events in Duchenne muscular dystrophy. PLoS One 2018;13(3):e0194283.
[49] Bonati U, Hafner P, Schadelin S, Schmid M, Naduvilekoot Devasia A, Schroeder J, et al. Quantitative muscle MRI: a powerful surrogate outcome measure in Duchenne muscular dystrophy. Neuromuscul Disord : NMD 2015 Sep;25(9):679–85.
[50] Forbes SC, Arora H, Willcocks RJ, Triplett WT, Rooney WD, Barnard AM, et al. Upper and lower extremities in duchenne muscular dystrophy evaluated with quantitative MRI and proton MR spectroscopy in a multicenter cohort. Radiology 2020 Jun;295(3):616–25.
[51] Prompers JJ, Jeneson JA, Drost MR, Oomens CC, Strijkers GJ, Nicolay K. Dynamic MRS and MRI of skeletal muscle function and biomechanics. NMR Biomed 2006 Nov;19(7):927–53.
[52] Carlier RY, Laforet P, Wary C, Mompoint D, Laloui K, Pellegrini N, et al. Whole-body muscle MRI in 20 patients suffering from late onset Pompe disease: involvement patterns. Neuromuscul Disord : NMD 2011 Nov;21(11):791–9.
[53] Hankiewicz K, Carlier RY, Lazaro L, Linzoain J, Barnerias C, Gomez-Andres D, et al. Whole-body muscle magnetic resonance imaging in SEPN1-related myopathy shows a homogeneous and recognizable pattern. Muscle Nerve 2015 Nov;52(5):728–35.
[54] Luo S, Zhu W, Yue D, Lin J, Wang Y, Zhu Z, et al. Muscle pathology and whole-body MRI in a polyglucosan myopathy associated with a novel glycogenin-1 mutation. Neuromuscul Disord : NMD 2015 Oct;25(10):780–5.
[55] Reeder SB, Hu HH, Sirlin CB. Proton density fat-fraction: a standardized MR-based biomarker of tissue fat concentration. J Magn Reson Imag 2012 Nov;36(5):1011–4.
[56] Hu HH, Li Y, Nagy TR, Goran MI, Nayak KS. Quantification of absolute fat mass by magnetic resonance imaging: a validation study against chemical analysis. Int J Basic Clin Res 2011;9(3):111–22.
[57] Hong CW, Mamidipalli A, Hooker JC, Hamilton G, Wolfson T, Chen DH, et al. MRI proton density fat fraction is robust across the biologically plausible range of triglyceride spectra in adults with nonalcoholic steatohepatitis. J Magn Reson Imag 2018 Apr;47(4):995–1002.
[58] Ren J, Dimitrov I, Sherry AD, Malloy CR. Composition of adipose tissue and marrow fat in humans by 1H NMR at 7 Tesla. J Lipid Res 2008 Sep;49(9):2055–62.
[59] Bray TJ, Chouhan MD, Punwani S, Bainbridge A, Hall-Craggs MA. Fat fraction mapping using magnetic resonance imaging: insight into pathophysiology. Br J Radiol 2018 Sep;91(1089):20170344.
[60] Grimm A, Meyer H, Nickel MD, Nittka M, Raithel E, Chaudry O, et al. A comparison between 6-point dixon MRI and MR spectroscopy to quantify muscle fat in the thigh of subjects with sarcopenia. J Frailty Aging 2019;8(1):21–6.
[61] Noble JJ, Keevil SF, Totman J, Charles-Edwards GD. In vitro and in vivo comparison of two-, three- and four-point Dixon techniques for clinical intramuscular fat quantification at 3 T. Br J Radiol 2014 Apr;87(1036):20130761.
[62] Grimm A, Meyer H, Nickel MD, Nittka M, Raithel E, Chaudry O, et al. Evaluation of 2-point, 3-point, and 6-point Dixon magnetic resonance imaging with flexible echo timing for muscle fat quantification. Eur J Radiol 2018 Jun;103:57–64.
[63] Borga M, West J, Bell JD, Harvey NC, Romu T, Heymsfield SB, et al. Advanced body composition assessment: from body mass index to body composition profiling. J Invest Med 2018 Jun;66(5):887–95.
[64] West J, Leinhard OD, Romu T, Collins R, Garratt S, Bell JD, et al. Feasibility of MR-based body composition analysis in large scale population studies. PLoS One 2016 Sep 23;(9):11.
[65] Diehl-Wiesenecker E, von Armin CA, Dupuis L, Muller HP, Ludolph AC, Kassubek J. Adipose tissue distribution in patients with alzheimer's disease: a whole body MRI case-control study. J Alzheim Dis : JAD. 2015;48(3):825–32.
[66] Kustner T, Hepp T, Fischer M, Schwartz M, Fritsche A, Haring HU, et al. Fully automated and standardized segmentation of adipose tissue compartments via deep learning in 3D whole-body MRI of epidemiologic cohort studies. Radiol Artif Intell 2020 Nov;2(6):e200010.
[67] Reyngoudt H, Marty B, Boisserie JM, Le Louer J, Koumako C, Baudin PY, et al. Global versus individual muscle segmentation to assess quantitative MRI-based fat fraction changes in neuromuscular diseases. Eur Radiol 2021 Jun;31(6):4264–76.
[68] Pinal-Fernandez I, Casal-Dominguez M, Carrino JA, Lahouti AH, Basharat P, Albayda J, et al. Thigh muscle MRI in immune-mediated necrotising myopathy: extensive oedema, early muscle damage and role of anti-SRP autoantibodies as a marker of severity. Ann Rheum Dis 2017 Apr;76(4):681–7.
[69] Pinal-Fernandez I, Casal-Dominguez M, Mammen AL. Immune-Mediated necrotizing myopathy. Curr Rheumatol Rep 2018 Mar 26;20(4):21.
[70] Arpan I, Forbes SC, Lott DJ, Senesac CR, Daniels MJ, Triplett WT, et al. T(2) mapping provides multiple approaches for the characterization of muscle involvement in neuromuscular diseases: a cross-sectional study of lower leg muscles in 5-15-year-old boys with Duchenne muscular dystrophy. NMR Biomed 2013 Mar;26(3):320–8.
[71] Carlier PG. Global T2 versus water T2 in NMR imaging of fatty infiltrated muscles: different methodology, different information and different implications. Neuromuscul Disord : NMD 2014 May;24(5):390–2.
[72] Gold GE, Han E, Stainsby J, Wright G, Brittain J, Beaulieu C. Musculoskeletal MRI at 3.0 T: relaxation times and image contrast. AJR Am J Roentgenol 2004 Aug;183(2):343–51.
[73] Azzabou N, Loureiro de Sousa P, Caldas E, Carlier PG. Validation of a generic approach to muscle water T2 determination at 3T in fat-infiltrated skeletal muscle. J Magn Reson Imag 2015 Mar;41(3):645–53.
[74] Mankodi A, Azzabou N, Bulea T, Reyngoudt H, Shimellis H, Ren Y, et al. Skeletal muscle water T2 as a biomarker of disease status and exercise effects in patients with Duchenne muscular dystrophy. Neuromuscul Disord : NMD 2017 Aug;27(8):705–14.
[75] Yao L, Gai N. Fat-corrected T2 measurement as a marker of active muscle disease in inflammatory myopathy. AJR Am J Roentgenol 2012 May;198(5):W475–81.

[76] Taylor DG, Bushell MC. The spatial-mapping of translational diffusion-coefficients by the nmr imaging technique. Phys Med Biol 1985;30(4):345–9.
[77] Soares JM, Marques P, Alves V, Sousa N. A hitchhiker's guide to diffusion tensor imaging. Front Neurosci-Switz. 2013;7.
[78] Damon BM. Effects of image noise in muscle diffusion tensor (DT)-MRI assessed using numerical simulations. Magn Reson Med 2008 Oct;60(4):934–44.
[79] Williams SE, Heemskerk AM, Welch EB, Li K, Damon BM, Park JH. Quantitative effects of inclusion of fat on muscle diffusion tensor MRI measurements. J Magn Reson Imag 2013 Nov;38(5):1292–7.
[80] Longwei X. Clinical application of diffusion tensor magnetic resonance imaging in skeletal muscle. Muscles Ligaments Tendons J 2012 Jan;2(1):19–24.
[81] Ponrartana S, Ramos-Platt L, Wren TA, Hu HH, Perkins TG, Chia JM, et al. Effectiveness of diffusion tensor imaging in assessing disease severity in Duchenne muscular dystrophy: preliminary study. Pediatr Radiol 2015 Apr;45(4):582–9.
[82] Li W, Zheng Y, Zhang W, Wang Z, Xiao J, Yuan Y. Progression and variation of fatty infiltration of the thigh muscles in Duchenne muscular dystrophy, a muscle magnetic resonance imaging study. Neuromuscul Disord : NMD 2015 May;25(5):375–80.
[83] Ai T, Yu K, Gao L, Zhang P, Goerner F, Runge VM, et al. Diffusion tensor imaging in evaluation of thigh muscles in patients with polymyositis and dermatomyositis. Br J Radiol 2014 Nov;87(1043):20140261.
[84] Wang F, Wu C, Sun C, Liu D, Sun Y, Wang Q, et al. Simultaneous multislice accelerated diffusion tensor imaging of thigh muscles in myositis. AJR Am J Roentgenol 2018 Oct;211(4):861–6.
[85] Qi J, Olsen NJ, Price RR, Winston JA, Park JH. Diffusion-weighted imaging of inflammatory myopathies: polymyositis and dermatomyositis. J Magn Reson Imag 2008 Jan;27(1):212–7.
[86] Farrow M, Biglands JD, Grainger AJ, O'Connor P, Hensor EMA, Ladas A, et al. Quantitative MRI in myositis patients: comparison with healthy volunteers and radiological visual assessment. Clin Radiol 2021 Jan;76(1):81 e1–e10.
[87] Li GD, Liang YY, Xu P, Ling J, Chen YM. Diffusion-tensor imaging of thigh muscles in duchenne muscular dystrophy: correlation of apparent diffusion coefficient and fractional anisotropy values with fatty infiltration. Am J Roentgenol 2016 Apr;206(4):867–70.
[88] McDowell AR, Feiweier T, Muntoni F, Hall MG, Clark CA. Clinically feasible diffusion MRI in muscle: time dependence and initial findings in Duchenne muscular dystrophy. Magn Reson Med 2021 Dec;86(6):3192–200.
[89] Froeling M, Nederveen AJ, Nicolay K, Strijkers GJ. DTI of human skeletal muscle: the effects of diffusion encoding parameters, signal-to-noise ratio and T2 on tensor indices and fiber tracts. NMR Biomed 2013 Nov;26(11):1339–52.
[90] Hooijmans MT, Damon BM, Froeling M, Versluis MJ, Burakiewicz J, Verschuuren JJ, et al. Evaluation of skeletal muscle DTI in patients with duchenne muscular dystrophy. NMR Biomed 2015 Nov;28(11):1589–97.
[91] Damon BM, Froeling M, Buck AKW, Oudeman J, Ding ZH, Nederveen AJ, et al. Skeletal muscle diffusion tensor-MRI fiber tracking: rationale, data acquisition and analysis methods, applications and future directions. NMR Biomed 2017 Mar;30(3).
[92] Oudeman J, Nederveen AJ, Strijkers GJ, Maas M, Luijten PR, Froeling M. Techniques and applications of skeletal muscle diffusion tensor imaging: a review. J Magn Reson Imag 2016 Apr;43(4):773–88.
[93] Martin-Noguerol T, Barousse R, Wessell DE, Rossi I, Luna A. A handbook for beginners in skeletal muscle diffusion tensor imaging: physical basis and technical adjustments. Eur Radiol 2022 May 12.
[94] Tan ET, Zochowski KC, Sneag DB. Diffusion MRI fiber diameter for muscle denervation assessment. Quant Imag Med Surg 2022 Jan;12(1):80–94.
[95] Edalati M, Hastings MK, Sorensen CJ, Zayed M, Mueller MJ, Hildebolt CF, et al. Diffusion tensor imaging of the calf muscles in subjects with and without diabetes mellitus. J Magn Reson Imag 2019 May;49(5):1285–95.
[96] Rehmann R, Schlaffke L, Froeling M, Kley RA, Kuhnle E, De Marees M, et al. Muscle diffusion tensor imaging in glycogen storage disease V (McArdle disease). Eur Radiol 2019 Jun;29(6):3224–32.
[97] Biglands JD, Grainger AJ, Robinson P, Tanner SF, Tan AL, Feiweier T, et al. MRI in acute muscle tears in athletes: can quantitative T2 and DTI predict return to play better than visual assessment? Eur Radiol 2020 Dec;30(12):6603–13.
[98] Giraudo C, Motyka S, Weber M, Karner M, Resinger C, Feiweier T, et al. Normalized STEAM-based diffusion tensor imaging provides a robust assessment of muscle tears in football players: preliminary results of a new approach to evaluate muscle injuries. Eur Radiol 2018 Jul;28(7):2882–9.
[99] Di Pietro G, Scimeca M, Iundusi R, Celi M, Gasbarra E, Tarantino U, et al. Differences between muscle from osteoporotic and osteoarthritic subjects: in vitro study by diffusion-tensor MRI and histological findings. Aging Clin Exp Res 2020 Dec;32(12):2489–99.
[100] Klupp E, Cervantes B, Schlaeger S, Inhuber S, Kreuzpointer F, Schwirtz A, et al. Paraspinal muscle DTI metrics predict muscle strength. J Magn Reson Imag 2019 Sep;50(3):816–23.
[101] Okamoto Y, Kemp GJ, Isobe T, Sato E, Hirano Y, Shoda J, et al. Changes in diffusion tensor imaging (DTI) eigenvalues of skeletal muscle due to hybrid exercise training. Magn Reson Imaging 2014 Dec;32(10):1297–300.
[102] Takao S, Kaneda M, Sasahara M, Takayama S, Matsumura Y, Okahisa T, et al. Diffusion tensor imaging (DTI) of human lower leg muscles: correlation between DTI parameters and muscle power with different ankle positions. Jpn J Radiol 2022 Sep;40(9):939–48.
[103] Keller S, Yamamura J, Sedlacik J, Wang ZJ, Gebert P, Starekova J, et al. Diffusion tensor imaging combined with T2 mapping to quantify changes in the skeletal muscle associated with training and endurance exercise in competitive triathletes. Eur Radiol 2020 May;30(5):2830–42.
[104] Yamauchi K, Someya K, Kato C, Kato T. The relationship between quadriceps femoris muscle function and MRI-derived water diffusion and adipose tissue measurements in young healthy males. J Magn Reson Imag 2022 Nov 7.
[105] Froeling M, Oudeman J, Strijkers GJ, Maas M, Drost MR, Nicolay K, et al. Muscle changes detected with diffusion-tensor imaging after long-distance running. Radiology 2015 Feb;274(2):548–62.
[106] Stavres J, Wang J, Sica CT, Blaha C, Herr M, Pai S, et al. Diffusion tensor imaging indices of acute muscle damage are augmented after exercise in peripheral arterial disease. Eur J Appl Physiol 2021 Sep;121(9):2595–606.
[107] Forsting J, Rehmann R, Froeling M, Vorgerd M, Tegenthoff M, Schlaffke L. Diffusion tensor imaging of the human thigh: consideration of DTI-based fiber tracking stop criteria. Magn Reson Mater Phy 2020 Jun;33(3):343–55.
[108] Cui C, Zhao Y, Cui D, Li N, Pan J, Shen W. In vivo evaluation of the levator ani muscle in primiparous women using diffusion tensor imaging and fiber tractography. Int J Gynaecol Obstet: the official organ of the International Federation of Gynaecology and Obstetrics 2022 Jun;157(3):663–70.
[109] Joshi D, Dewald JPA, Ingo C. Development of DTI based probabilistic tractography methods to characterize arm muscle architecture in individuals post hemiparetic stroke. Annu Int Conf IEEE Eng Med Biol Soc 2021 Nov;2021:3451–4.
[110] Sugano T, Yoda N, Ogawa T, Hashimoto T, Shobara K, Niizuma K, et al. Application of diffusion tensor imaging fiber tractography for human masseter muscle. Tohoku J Exp Med 2022 Feb;256(2):151–60.
[111] Wada K, Hashimoto T, Miyagi R, Sakai T, Sairyo K. Diffusion tensor imaging and tractography of the sciatic nerve: assessment of fractional anisotropy and apparent diffusion coefficient values relative to the piriformis muscle, a preliminary study. Skeletal Radiol 2017 Mar;46(3):309–14.
[112] Yokohama T, Iwasaki M, Oura D, Furuya S, Niiya Y. Increased muscle fiber fractional anisotropy value using diffusion tensor imaging after compression without fiber injury. Acta Radiol 2021 Dec 2:2841851211058282.
[113] Weber MA, Nagel AM, Kan HE, Wattjes MP. Quantitative imaging in muscle diseases with focus on non-proton MRI and other advanced MRI techniques. Semin Muscoskel Radiol 2020 Aug;24(4):402–12.
[114] Donahue KM, Weisskoff RM, Parmelee DJ, Callahan RJ, Wilkinson RA, Mandeville JB, et al. Dynamic Gd-DTPA enhanced MRI measurement of tissue cell volume fraction. Magn Reson Med 1995 Sep;34(3):423–32.
[115] Nagel AM, Amarteifio E, Lehmann-Horn F, Jurkat-Rott K, Semmler W, Schad LR, et al. 3 Tesla sodium inversion recovery magnetic resonance imaging allows for improved visualization of intracellular sodium content changes in muscular channelopathies. Invest Radiol 2011 Dec;46(12):759–66.
[116] Constantinides CD, Gillen JS, Boada FE, Pomper MG, Bottomley PA. Human skeletal muscle: sodium MR imaging and quantification-potential applications in exercise and disease. Radiology 2000 Aug;216(2):559–68.
[117] Kopp C, Linz P, Dahlmann A, Hammon M, Jantsch J, Muller DN, et al. 23Na magnetic resonance imaging-determined tissue sodium in healthy subjects and hypertensive patients. Hypertension 2013 Mar;61(3):635–40.
[118] Gerhalter T, Gast LV, Marty B, Martin J, Trollmann R, Schussler S, et al. 23) Na MRI depicts early changes in ion homeostasis in skeletal muscle tissue of patients with duchenne muscular dystrophy. J Magn Reson Imag 2019 Feb 4.
[119] Nagel AM, Lehmann-Horn F, Weber MA, Jurkat-Rott K, Wolf MB, Radbruch A, et al. In vivo 35Cl MR imaging in humans: a feasibility study. Radiology 2014 May;271(2):585–95.
[120] Umathum R, Rosler MB, Nagel AM. In vivo 39K MR imaging of human muscle and brain. Radiology 2013 Nov;269(2):569–76.
[121] Gast LV, Volker S, Utzschneider M, Linz P, Wilferth T, Muller M, et al. Combined imaging of potassium and sodium in human skeletal muscle tissue at 7 T. Magn Reson Med 2021 Jan;85(1):239–53.
[122] Weber MA, Nagel AM, Marschar AM, Glemser P, Jurkat-Rott K, Wolf MB, et al. 7-T (35)Cl and (23)Na MR imaging for detection of mutation-dependent alterations in muscular edema and fat fraction with sodium and chloride concentrations in muscular periodic paralyses. Radiology 2016 Oct;281(1):326.
[123] Gast LV, Baier LM, Meixner CR, Chaudry O, Engelke K, Uder M, et al. MRI of potassium and sodium enables comprehensive analysis of ion perturbations in skeletal muscle tissue after eccentric exercise. Invest Radiol 2022 Oct 21.
[124] Uffmann K, Ladd ME. Actuation systems for MR elastography: design and applications. IEEE Eng Med Biol Mag 2008 May-Jun;27(3):28–34.
[125] Manduca A, Bayly PJ, Ehman RL, Kolipaka A, Royston TJ, Sack I, et al. MR elastography: principles, guidelines, and terminology. Magn Reson Med 2021 May;85(5):2377–90.
[126] Bensamoun SF, Charleux F, Debernard L, Themar-Noel C, Voit T. Elastic properties of skeletal muscle and subcutaneous tissues in Duchenne muscular dystrophy by magnetic resonance elastography (MRE): a feasibility study. IRBM 2015;36(1):4–9.
[127] Chakouch MK, Charleux F, Bensamoun SF. Quantifying the elastic property of nine thigh muscles using magnetic resonance elastography. PLoS One 2015;10(9):e0138873.
[128] Ogier AC, Hostin MA, Bellemare ME, Bendahan D. Overview of MR image segmentation strategies in neuromuscular disorders. Front Neurol 2021;12:625308.
[129] Pons C, Borotikar B, Garetier M, Burdin V, Ben Salem D, Lempereur M, et al. Quantifying skeletal muscle volume and shape in humans using MRI: a systematic review of validity and reliability. PLoS One 2018;13(11):e0207847.
[130] Dahlqvist JR, Widholm P, Leinhard OD, Vissing J. MRI in neuromuscular diseases: an emerging diagnostic tool and biomarker for prognosis and efficacy. Ann Neurol 2020 Oct;88(4):669–81.
[131] Diaz-Manera J, Walter G, Straub V. Skeletal muscle magnetic resonance imaging in Pompe disease. Muscle Nerve 2021 May;63(5):640–50.

[132] Barra V, Boire JY. Segmentation of fat and muscle from MR images of the thigh by a possibilistic clustering algorithm. Comput Methods Progr Biomed 2002 Jun; 68(3):185–93.
[133] Positano V, Christiansen T, Santarelli MF, Ringgaard S, Landini L, Gastaldelli A. Accurate segmentation of subcutaneous and intermuscular adipose tissue from MR images of the thigh. J Magn Reson Imag 2009 Mar;29(3):677–84.
[134] Yang YX, Chong MS, Lim WS, Tay L, Yew S, Yeo A, et al. Validity of estimating muscle and fat volume from a single MRI section in older adults with sarcopenia and sarcopenic obesity. Clin Radiol 2017 May;72(5):427. e9- e14.
[135] Valentinitsch A, Karampinos DC, Alizai H, Subburaj K, Kumar D, Link TM, et al. Automated unsupervised multi-parametric classification of adipose tissue depots in skeletal muscle. J Magn Reson Imag 2013 Apr;37(4):917–27.
[136] Wang F, Zhou S, Hou B, Santini F, Yuan L, Guo Y, et al. Assessment of idiopathic inflammatory myopathy using a deep learning method for muscle T2 mapping segmentation. Eur Radiol 2022 Nov 18:1–8.
[137] Chaudry O, Friedberger A, Grimm A, Uder M, Nagel AM, Kemmler W, et al. Segmentation of the fascia lata and reproducible quantification of intermuscular adipose tissue (IMAT) of the thigh. Magma 2021 Jun;34(3):367–76.
[138] Kowacs W, Liu C, Summers RM, Yao J. Identification of muscle and subcutaneous and intermuscular adipose tissue on thigh MRI of muscular dystrophy. EEE 13th International Symposium on Biomedical Imaging (ISBI). Prague: IEEE; 2016. p. 176–9.
[139] Kemnitz J, Baumgartner CF, Eckstein F, Chaudhari A, Ruhdorfer A, Wirth W, et al. Clinical evaluation of fully automated thigh muscle and adipose tissue segmentation using a U-Net deep learning architecture in context of osteoarthritic knee pain. Magma 2020 Aug;33(4):483–93.
[140] Amer R, Nassar J, Trabelsi A, Bendahan D, Greenspan H, Ben-Eliezer N. Quantification of intra-muscular adipose infiltration in calf/thigh MRI using fully and weakly supervised semantic segmentation. Bioengineering (Basel) 2022 Jul 14;9(7).
[141] Barnouin Y, Butler-Browne G, Voit T, Reversat D, Azzabou N, Leroux G, et al. Manual segmentation of individual muscles of the quadriceps femoris using MRI: a reappraisal. J Magn Reson Imag 2014 Jul;40(1):239–47.
[142] Holmback AM, Askaner K, Holtas S, Downham D, Lexell J. Assessment of contractile and noncontractile components in human skeletal muscle by magnetic resonance imaging. Muscle Nerve 2002 Feb;25(2):251–8.
[143] Commean PK, Tuttle LJ, Hastings MK, Strube MJ, Mueller MJ. Magnetic resonance imaging measurement reproducibility for calf muscle and adipose tissue volume. J Magn Reson Imag 2011 Dec;34(6):1285–94.
[144] Kiefer LS, Fabian J, Lorbeer R, Machann J, Storz C, Kraus MS, et al. Inter- and intra-observer variability of an anatomical landmark-based, manual segmentation method by MRI for the assessment of skeletal muscle fat content and area in subjects from the general population. Br J Radiol 2018 Sep;91(1089):20180019.
[145] Ogier A, Sdika M, Foure A, Le Troter A, Bendahan D. Individual muscle segmentation in MR images: a 3D propagation through 2D non-linear registration approaches. Annu Int Conf IEEE Eng Med Biol Soc 2017:317–20. 2017 Jul.
[146] Ogier AC, Heskamp L, Michel CP, Foure A, Bellemare ME, Le Troter A, et al. A novel segmentation framework dedicated to the follow-up of fat infiltration in individual muscles of patients with neuromuscular disorders. Magn Reson Med 2020 May;83(5):1825–36.
[147] Sasaki T, Yoshimura N, Hashizume H, Yamada H, Oka H, Matsudaira K, et al. MRI-defined paraspinal muscle morphology in Japanese population: the Wakayama Spine Study. PLoS One 2017;12(11):e0187765.
[148] Kim JY, Chae SU, Kim GD, Cha MS. Changes of paraspinal muscles in postmenopausal osteoporotic spinal compression fractures: magnetic resonance imaging study. J Bone Metab 2013 Nov;20(2):75–81.
[149] Rummens S, Bosch S, Dierckx S, Vanmechelen A, Peeters R, Brumagne S, et al. Reliability and agreement of lumbar multifidus volume and fat fraction quantification using magnetic resonance imaging. Musculoskelet Sci Pract 2022 Jun;59:102532.
[150] Tagliaferri SD, Miller CT, Ford JJ, Hahne AJ, Main LC, Rantalainen T, et al. Randomized trial of general strength and conditioning versus motor control and manual therapy for chronic low back pain on physical and self-report outcomes. J Clin Med 2020 Jun 3;9(6).
[151] Sions JM, Elliott JM, Pohlig RT, Hicks GE. Trunk muscle characteristics of the multifidi, erector spinae, psoas, and quadratus lumborum in older adults with and without chronic low back pain. J Orthop Sports Phys Ther 2017 Mar;47(3):173–9.
[152] Tustison NJ, Avants BB, Cook PA, Zheng Y, Egan A, Yushkevich PA, et al. N4ITK: improved N3 bias correction. IEEE Trans Med Imag 2010 Jun;29(6):1310–20.
[153] Borga M. MRI adipose tissue and muscle composition analysis-a review of automation techniques. Br J Radiol 2018;91(1089).
[154] Ghasemikaram M, Chaudry O, Nagel AM, Uder M, Jakob F, Kemmler W, et al. Effects of 16 months of high intensity resistance training on thigh muscle fat infiltration in elderly men with osteosarcopenia. Geroscience 2021 Apr;43(2): 607–17.
[155] Kullberg J, Johansson L, Ahlstrom H, Courivaud F, Koken P, Eggers H, et al. Automated assessment of whole-body adipose tissue depots from continuously moving bed MRI: a feasibility study. J Magn Reson Imag 2009 Jul;30(1):185–93.
[156] Linge J, Petersson M, Forsgren MF, Sanyal AJ, Dahlqvist Leinhard O. Adverse muscle composition predicts all-cause mortality in the UK Biobank imaging study. J Cachexia Sarcopenia Muscle 2021 Dec;12(6):1513–26.
[157] Fortin M, Omidyeganeh M, Battie MC, Ahmad O, Rivaz H. Evaluation of an automated thresholding algorithm for the quantification of paraspinal muscle composition from MRI images. Biomed Eng Online 2017 May 22;16(1):61.
[158] Mattei JP, Fur YL, Cuge N, Guis S, Cozzone PJ, Bendahan D. Segmentation of fascias, fat and muscle from magnetic resonance images in humans: the DISPIMAG software. Magma 2006 Nov;19(5):275–9.
[159] Ogawa M, Lester R, Akima H, Gorgey AS. Quantification of intermuscular and intramuscular adipose tissue using magnetic resonance imaging after neurodegenerative disorders. Neural Regeneration Research 2017 Dec;12(12): 2100–5.
[160] Lareau-Trudel E, Le Troter A, Ghattas B, Pouget J, Attarian S, Bendahan D, et al. Muscle quantitative MR imaging and clustering analysis in patients with facioscapulohumeral muscular dystrophy type 1. PLoS One 2015;10(7):e0132717.
[161] Orgiu S, Lafortuna CL, Rastelli F, Cadioli M, Falini A, Rizzo G. Automatic muscle and fat segmentation in the thigh from T1-Weighted MRI. J Magn Reson Imag 2016 Mar;43(3):601–10.
[162] Gadermayr M, Disch C, Muller M, Merhof D, Gess B. A comprehensive study on automated muscle segmentation for assessing fat infiltration in neuromuscular diseases. Magn Reson Imaging 2018 May;48:20–6.
[163] Alic L, Griffin JFt, Eresen A, Kornegay JN, Ji JX. Using MRI to quantify skeletal muscle pathology in Duchenne muscular dystrophy: a systematic mapping review. Muscle Nerve 2021 Jul;64(1):8–22.
[164] Burakiewicz J, Sinclair CDJ, Fischer D, Walter GA, Kan HE, Hollingsworth KG. Quantifying fat replacement of muscle by quantitative MRI in muscular dystrophy. J Neurol 2017 Oct;264(10):2053–67.
[165] Carlier PG, Marty B, Scheidegger O, Loureiro de Sousa P, Baudin PY, Snezhko E, et al. Skeletal muscle quantitative nuclear magnetic resonance imaging and spectroscopy as an outcome measure for clinical trials. J Neuromuscul Dis 2016 Mar 3;3(1):1–28.
[166] Chrzanowski SM, Darras BT, Rutkove SB. The value of imaging and composition-based biomarkers in duchenne muscular dystrophy clinical trials. Neurotherapeutics 2020 Jan;17(1):142–52.
[167] Kriss A, Jenkins T. Muscle MRI in motor neuron diseases: a systematic review. Amyotroph Lateral Scler Frontotemporal Degener 2022 May;23(3–4):161–75.
[168] Reginster JY, Beaudart C, Al-Daghri N, Avouac B, Bauer J, Bere N, et al. Update on the ESCEO recommendation for the conduct of clinical trials for drugs aiming at the treatment of sarcopenia in older adults. Aging Clin Exp Res 2021 Jan;33(1): 3–17.
[169] Ropars J, Gravot F, Ben Salem D, Rousseau F, Brochard S, Pons C. Muscle MRI: a biomarker of disease severity in Duchenne muscular dystrophy? A systematic review. Neurology 2020 Jan 21;94(3):117–33.
[170] Ramirez-Velez R, Ezzatvar Y, Izquierdo M, Garcia-Hermoso A. Effect of exercise on myosteatosis in adults: a systematic review and meta-analysis. J Appl Physiol 2021 Jan 1;130(1):245–55. 1985.
[171] Arpan I, Willcocks RJ, Forbes SC, Finkel RS, Lott DJ, Rooney WD, et al. Examination of effects of corticosteroids on skeletal muscles of boys with DMD using MRI and. MRS. Neurology. 2014 Sep 9;83(11):974–80.
[172] Wagner KR, Abdel-Hamid HZ, Mah JK, Campbell C, Guglieri M, Muntoni F, et al. Randomized phase 2 trial and open-label extension of domagrozumab in Duchenne muscular dystrophy. Neuromuscul Disord : NMD 2020 Jun;30(6): 492–502.
[173] Wagner KR, Fleckenstein JL, Amato AA, Barohn RJ, Bushby K, Escolar DM, et al. A phase I/IItrial of MYO-029 in adult subjects with muscular dystrophy. Ann Neurol 2008 May;63(5):561–71.
[174] Willcocks RJ, Rooney WD, Triplett WT, Forbes SC, Lott DJ, Senesac CR, et al. Multicenter prospective longitudinal study of magnetic resonance biomarkers in a large duchenne muscular dystrophy cohort. Ann Neurol 2016 Apr;79(4):535–47.
[175] Lokken N, Revsbech KL, Jacobsen LN, Martinuzzi A, Martin MA, Diaz-Manera J, et al. Muscle MRI in McArdle disease: a European multicenter observational study. Neurology 2022 Jul 19.
[176] Willis TA, Hollingsworth KG, Coombs A, Sveen ML, Andersen S, Stojkovic T, et al. Quantitative muscle MRI as an assessment tool for monitoring disease progression in LGMD2I: a multicentre longitudinal study. PLoS One 2013;8(8):e70993.
[177] Gluer CC, Blake G, Lu Y, Blunt BA, Jergas M, Genant HK. Accurate assessment of precision errors: how to measure the reproducibility of bone densitometry techniques. Osteoporos Int 1995;5(4):262–70.
[178] Borga M, Ahlgren A, Romu T, Widholm P, Dahlqvist Leinhard O, West J. Reproducibility and repeatability of MRI-based body composition analysis. Magn Reson Med 2020 Dec;84(6):3146–56.
[179] Johnston JD, Liao L, Dolovich AT, Leswick DA, Kontulainen SA. Magnetic resonance imaging of bone and muscle traits at the hip: an in vivo precision study. J Musculoskelet Neuronal Interact 2014 Mar;14(1):104–10.
[180] Widholm P, Ahlgren A, Karlsson M, Romu T, Tawil R, Wagner KR, et al. Quantitative muscle analysis in facioscapulohumeral muscular dystrophy using whole-body fat-referenced MRI: protocol development, multicenter feasibility, and repeatability. Muscle & nerve; 2022 May 18.
[181] Middleton MS, Haufe W, Hooker J, Borga M, Leinhard OD, Romu T, et al. Quantifying abdominal adipose tissue and thigh muscle volume and hepatic proton density fat fraction: repeatability and accuracy of an MR imaging-based, semiautomated analysis method. Radiology 2017 May;283(2):438–49.
[182] Grimm A, Meyer H, Nickel MD, Nittka M, Raithel E, Chaudry O, et al. Repeatability of Dixon magnetic resonance imaging and magnetic resonance spectroscopy for quantitative muscle fat assessments in the thigh. J Cachexia Sarcopenia Muscle 2018 Dec;9(6):1093–100.
[183] Schlaffke L, Rehmann R, Rohm M, Otto LAM, de Luca A, Burakiewicz J, et al. Multi-center evaluation of stability and reproducibility of quantitative MRI measures in healthy calf muscles. NMR Biomed 2019 Sep;32(9):e4119.
[184] Morrow JM, Sinclair CD, Fischmann A, Reilly MM, Hanna MG, Yousry TA, et al. Reproducibility, and age, body-weight and gender dependency of candidate

skeletal muscle MRI outcome measures in healthy volunteers. Eur Radiol 2014 Jul; 24(7):1610–20.
[185] Naraghi A, White LM. Three-dimensional MRI of the musculoskeletal system. AJR Am J Roentgenol 2012 Sep;199(3):W283–93.
[186] Tomlinson OW, Barker AR, Fulford J, Wilson P, Oades PJ, Williams CA. Quantification of thigh muscle volume in children and adolescents using magnetic resonance imaging. Eur J Sport Sci 2020 Oct;20(9):1215–24.
[187] Fatehi F, Salort-Campana E, Le Troter A, Bendahan D, Attarian S. Muscle MRI of facioscapulohumeral dystrophy (FSHD): a growing demand and a promising approach. Rev Neurol 2016 Oct;172(10):566–71.
[188] Hu HH, Yokoo T, Bashir MR, Sirlin CB, Hernando D, Malyarenko D, et al. Linearity and bias of proton density fat fraction as a quantitative imaging biomarker: a multicenter, multiplatform, multivendor phantom study. Radiology 2021 Mar; 298(3):640–51.
[189] Crawford RJ, Filli L, Elliott JM, Nanz D, Fischer MA, Marcon M, et al. Age- and level-dependence of fatty infiltration in lumbar paravertebral muscles of healthy volunteers. AJNR Am J Neuroradiol 2016 Apr;37(4):742–8.
[190] Dallaway A, Hattersley J, Diokno M, Tallis J, Renshaw D, Wilson A, et al. Age-related degeneration of lumbar muscle morphology in healthy younger versus older men. Aging Male 2020 Dec;23(5):1583–97.
[191] Farrow M, Grainger AJ, Tan AL, Buch MH, Emery P, Ridgway JP, et al. Normal values and test-retest variability of stimulated-echo diffusion tensor imaging and fat fraction measurements in the muscle. Br J Radiol 2019 Sep;92(1101): 20190143.
[192] Hogrel JY, Barnouin Y, Azzabou N, Butler-Browne G, Voit T, Moraux A, et al. NMR imaging estimates of muscle volume and intramuscular fat infiltration in the thigh: variations with muscle, gender, and age. Age (Dordr). 2015 Jun;37(3):9798.
[193] Yoon MA, Hong SJ, Ku MC, Kang CH, Ahn KS, Kim BH. Multiparametric MR imaging of age-related changes in healthy thigh muscles. Radiology 2018 Apr; 287(1):235–46.
[194] Engelke K, Ghasemikaram M, Chaudry O, Uder M, Nagel AM, Jakob F, et al. The effect of ageing on fat infiltration of thigh and paraspinal muscles in men. Aging Clin Exp Res 2022 Sep;34(9):2089–98.
[195] Dixon WT. Simple proton spectroscopic imaging. Radiology 1984;153(1):189–94.
[196] Ma J. Dixon techniques for water and fat imaging. J Magn Reson Imag 2008 Sep; 28(3):543–58.
[197] Reeder SB, Cruite I, Hamilton G, Sirlin CB. Quantitative assessment of liver fat with magnetic resonance imaging and spectroscopy. J Magn Reson Imag 2011 Oct; 34(4):729–49.
[198] Liu CY, McKenzie CA, Yu H, Brittain JH, Reeder SB. Fat quantification with IDEAL gradient echo imaging: correction of bias from T(1) and noise. Magn Reson Med 2007 Aug;58(2):354–64.
[199] Karlsson A, Peolsson A, Romu T, Dahlqvist Leinhard O, Spetz Holm AC, Thorell S, et al. The effect on precision and T1 bias comparing two flip angles when estimating muscle fat infiltration using fat-referenced chemical shift-encoded imaging. NMR Biomed 2021 Nov;34(11):e4581.
[200] Peterson P, Romu T, Brorson H, Dahlqvist Leinhard O, Mansson S. Fat quantification in skeletal muscle using multigradient-echo imaging: comparison of fat and water references. J Magn Reson Imag 2016 Jan;43(1):203–12.
[201] Hernando D, Hines CD, Yu H, Reeder SB. Addressing phase errors in fat-water imaging using a mixed magnitude/complex fitting method. Magn Reson Med 2012 Mar;67(3):638–44.
[202] Bydder M, Yokoo T, Yu H, Carl M, Reeder SB, Sirlin CB. Constraining the initial phase in water-fat separation. Magn Reson Imaging 2011 Feb;29(2):216–21.
[203] Yu H, Shimakawa A, McKenzie CA, Lu W, Reeder SB, Hinks RS, et al. Phase and amplitude correction for multi-echo water-fat separation with bipolar acquisitions. J Magn Reson Imag 2010 May;31(5):1264–71.
[204] Carson BW, Xiang QS. Fat suppression using direct phase encoding: musculoskeletal applications using MR imaging. AJR Am J Roentgenol 1999 Jul; 173(1):230–3.
[205] Xiang QS. Two-point water-fat imaging with partially-opposed-phase (POP) acquisition: an asymmetric Dixon method. Magn Reson Med 2006 Sep;56(3): 572–84.
[206] Glover GH. Multipoint Dixon technique for water and fat proton and susceptibility imaging. J Magn Reson Imag 1991 Sep-Oct;1(5):521–30.
[207] Glover GH, Schneider E. Three-point Dixon technique for true water/fat decomposition with B0 inhomogeneity correction. Magn Reson Med 1991 Apr; 18(2):371–83.
[208] Reeder SB, McKenzie CA, Pineda AR, Yu H, Shimakawa A, Brau AC, et al. Water-fat separation with IDEAL gradient-echo imaging. J Magn Reson Imag 2007 Mar; 25(3):644–52.
[209] Wang Y, Li D, Haacke EM, Brown JJ. A three-point Dixon method for water and fat separation using 2D and 3D gradient-echo techniques. J Magn Reson Imag 1998 May-Jun;8(3):703–10.
[210] Reeder SB, Pineda AR, Wen Z, Shimakawa A, Yu H, Brittain JH, et al. Iterative decomposition of water and fat with echo asymmetry and least-squares estimation (IDEAL): application with fast spin-echo imaging. Magn Reson Med 2005 Sep; 54(3):636–44.
[211] Berglund J, Ahlstrom H, Johansson L, Kullberg J. Two-point dixon method with flexible echo times. Magn Reson Med 2011 Apr;65(4):994–1004.
[212] Eggers H, Brendel B, Duijndam A, Herigault G. Dual-echo Dixon imaging with flexible choice of echo times. Magn Reson Med 2011 Jan;65(1):96–107.
[213] Kukuk GM, Hittatiya K, Sprinkart AM, Eggers H, Gieseke J, Block W, et al. Comparison between modified Dixon MRI techniques, MR spectroscopic relaxometry, and different histologic quantification methods in the assessment of hepatic steatosis. Eur Radiol 2015 Oct;25(10):2869–79.
[214] Bydder M, Yokoo T, Hamilton G, Middleton MS, Chavez AD, Schwimmer JB, et al. Relaxation effects in the quantification of fat using gradient echo imaging. Magn Reson Imaging 2008 Apr;26(3):347–59.
[215] Chebrolu VV, Hines CD, Yu H, Pineda AR, Shimakawa A, McKenzie CA, et al. Independent estimation of T*2 for water and fat for improved accuracy of fat quantification. Magn Reson Med 2010 Apr;63(4):849–57.
[216] Yu H, Shimakawa A, McKenzie CA, Brodsky E, Brittain JH, Reeder SB. Multiecho water-fat separation and simultaneous R2* estimation with multifrequency fat spectrum modeling. Magn Reson Med 2008 Nov;60(5):1122–34.
[217] Zhong X, Nickel MD, Kannengiesser SA, Dale BM, Kiefer B, Bashir MR. Liver fat quantification using a multi-step adaptive fitting approach with multi-echo GRE imaging. Magn Reson Med 2014 Nov;72(5):1353–65.
[218] Hines CD, Yu H, Shimakawa A, McKenzie CA, Brittain JH, Reeder SB. T1 independent, T2* corrected MRI with accurate spectral modeling for quantification of fat: validation in a fat-water-SPIO phantom. J Magn Reson Imag 2009 Nov;30(5):1215–22.
[219] Lebel RM, Wilman AH. Transverse relaxometry with stimulated echo compensation. Magn Reson Med 2010 Oct;64(4):1005–14.
[220] Marty B, Baudin PY, Reyngoudt H, Azzabou N, Araujo EC, Carlier PG, et al. Simultaneous muscle water T2 and fat fraction mapping using transverse relaxometry with stimulated echo compensation. NMR Biomed 2016 Apr;29(4): 431–43.
[221] Santini F, Deligianni X, Paoletti M, Solazzo F, Weigel M, de Sousa PL, et al. Fast open-source toolkit for water T2 mapping in the presence of fat from multi-echo spin-echo acquisitions for muscle MRI. Front Neurol 2021;12:630387.
[222] Keene KR, Beenakker JM, Hooijmans MT, Naarding KJ, Niks EH, Otto LAM, et al. T2 relaxation-time mapping in healthy and diseased skeletal muscle using extended phase graph algorithms. Magn Reson Med 2020 Nov;84(5):2656–70.
[223] Basser PJ, Jones DK. Diffusion-tensor MRI: theory, experimental design and data analysis - a technical review. NMR Biomed 2002 Nov-Dec;15(7–8):456–67.